A&A, 684, A149 (2024)
https://doi.org/10.1051/0004-6361/202348794

Astronomy & Astrophysics

Spectrum and energy levels of the low-lying configurations of Nd III*

M. Ding[1], A. N. Ryabtsev[2], E. Y. Kononov[2], T. Ryabchikova[3], C. P. Clear[1], F. Concepcion[1], and J. C. Pickering[1]

[1] Physics Department, Imperial College London, Prince Consort Road, London SW7 2AZ, UK
e-mail: milan.ding15@imperial.ac.uk
[2] Institute of Spectroscopy, Russian Academy of Sciences, Troitsk, Moscow 108840, Russia
[3] Institute of Astronomy, Russian Academy of Sciences, Pyatnitskaya 48, Moscow 119017, Russia

Received 30 November 2023 / Accepted 27 January 2024

ABSTRACT

Aims. Our goal is to accurately determine bound-to-bound transition wavelengths and energy levels of the low-lying open-shell configurations $4f^4$, $4f^3 5d$, $4f^3 6s$, and $4f^3 6p$ of doubly ionised neodymium (Nd III) through high-resolution spectroscopy and semi-empirical calculations.

Methods. The emission spectra of neodymium (Nd, $Z = 60$) were recorded using Penning and hollow cathode discharge lamps in the region 11 500–54 000 cm^{-1} (8695–1852 Å) by Fourier transform spectroscopy at resolving powers up to 10^6. Wavenumber measurements were accurate to a few 10^{-3} cm^{-1}. Grating spectroscopy of Nd vacuum sliding sparks and stellar spectra were used to aid line and energy level identification. For the analysis, new Nd III atomic structure and transition probability calculations were carried out using the Cowan code parameterised by newly established levels.

Results. The classification of 432 transitions of Nd III from the Penning lamp spectra resulted in the determination of 144 energy levels of the $4f^4$, $4f^3 5d$, $4f^3 6s$, and $4f^3 6p$ configurations of Nd III, 105 of which were experimentally established for the first time. Of the 40 previously published Nd III levels, one was revised and 39 were confirmed.

Conclusions. The results will not only benchmark and improve future semi-empirical atomic structure calculations of Nd III, but also enable more reliable astrophysical applications of Nd III, such as abundance analyses of kilonovae and chemically peculiar stars, and studies of pulsational wave propagation in these stars.

Key words. atomic data – line: identification – methods: data analysis – methods: laboratory: atomic – stars: abundances – stars: chemically peculiar

1. Introduction

The accuracy and availability of atomic data are crucial in analyses of astrophysical spectra obtained by modern ground- and space-based telescopes. The lanthanide elements (Z = 57–71) are of great interest in studies of nucleosynthesis, stellar evolution, and Galactic chemical evolution due to their unsettled origins as of yet. Lines from singly and doubly ionised lanthanide species are present in spectra of hot chemically peculiar stars in large quantities; for example, readers can refer to Przybylski's star (Przybylski 1977; Cowley et al. 2000). Numerous investigations on AT2017gfo (e.g. Valenti et al. 2017; Coulter et al. 2017), the electromagnetic counterpart of the neutron star merger event GW170817 (Abbott et al. 2017), indicated significant dependence of the kilonova opacity on lanthanide abundances (e.g. Kasen et al. 2013; Tanaka & Hotokezaka 2013; Smartt et al. 2017; Tanaka et al. 2018; Watson et al. 2019; Even et al. 2020; Domoto et al. 2022). However, the need for more extensive and accurate heavy element atomic data was almost always emphasised as the limitation to more detailed kilonova modelling. Much effort has been made to address this by means of large-scale atomic structure calculations of heavy elements (e.g. Kasen et al. 2013; Fontes et al. 2020; Tanaka et al. 2020). Nevertheless, reliable identifications of kilonova spectral features are still hindered by the incompleteness of experimental atomic data and the insufficient accuracies of theoretical calculations (Tanaka et al. 2020).

Despite the astrophysical interest in lanthanide spectral data, progress in obtaining accurate experimental energy levels and transition wavelengths of these elements is slow. Empirical investigations of atomic structures of the lanthanides are challenging due to their extremely complex and line-rich spectra owing to their open 4f subshells. Amongst the first few doubly ionised lanthanide elements, the spectrum of doubly ionised neodymium (Nd III, Z = 60) is one of the most poorly known ones, with only 40 experimental energy levels established previously by Ryabchikova et al. (2006).

In this paper, we address the need for accurate lanthanide atomic data in astronomy, particularly for Nd III, primarily by Fourier transform (FT) spectroscopy of a Penning discharge lamp (e.g. Finley et al. 1979; Heise et al. 1994) within the region 11 500–54 000 cm^{-1} (8695–1852 Å) using pure Nd cathodes. FT spectroscopy is capable of measuring spectra across a wide spectral range with high spectral resolution, which is ideal for investigating complex atomic spectra spanning from the IR to UV. At present, FT spectroscopy remains one of the best methods for extensive atomic structure analysis. Recent examples include: Mn II by Liggins et al. (2021), Ni II by Clear et al. (2022), and Zr I–II by Lawler et al. (2022).

* Full Tables 1 and 5–7 are available at the CDS via anonymous ftp to cdsarc.cds.unistra.fr (130.79.128.5) or via https://cdsarc.cds.unistra.fr/viz-bin/cat/J/A+A/684/A149

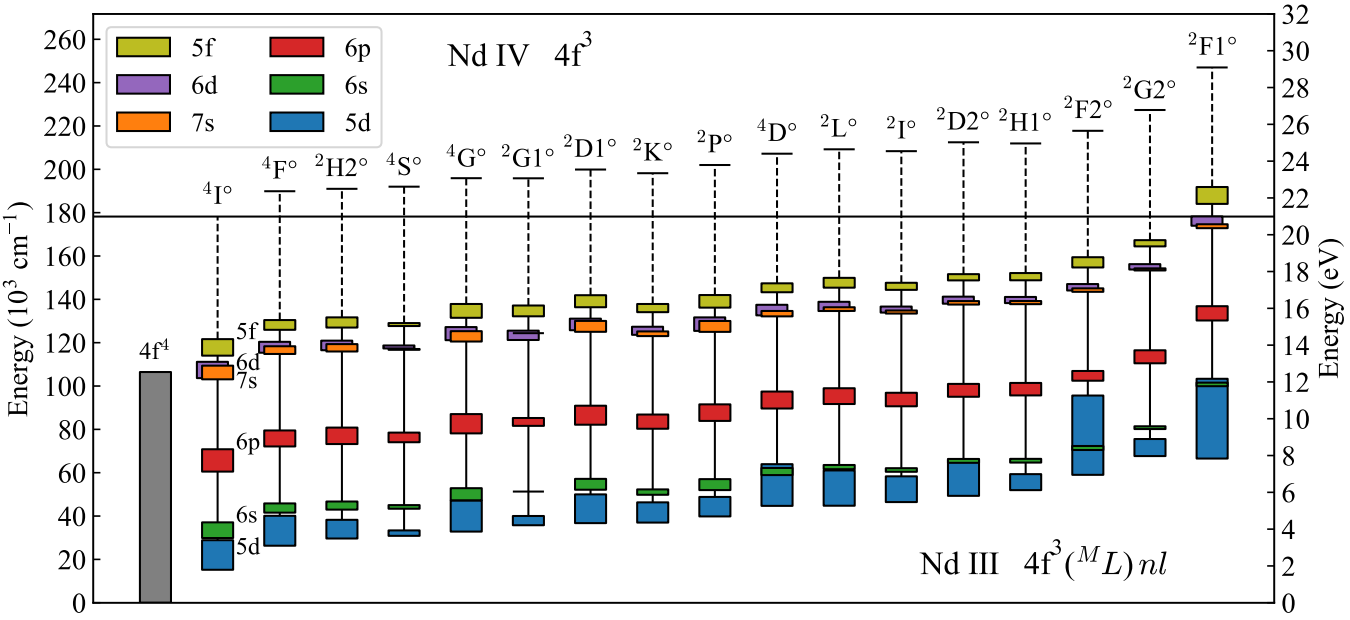

Fig. 1. Gross atomic structure of Nd III arising from the excitation of one 4f electron, $4f^3(^ML)nl$ for nl = 5d, 6s, 6p, 7s, 6d, and 5f, in relation with the *LS* terms of the Nd IV ground configuration $4f^3$. All levels are labelled according to the configurations and parent terms of their leading eigenvector components calculated in the present work using the Cowan code. The extent of each box merely shows the range of level energies within a given $4f^3(^ML)nl$ sub-configuration. The Nd III ionisation potential (shown by the horizontal black line) is from Johnson & Nelson (2017) and the Nd IV $4f^3$ term energies are from Wyart et al. (2007).

We present the empirical spectrum analysis for 144 energy levels of the $4f^4$, $4f^35d$, $4f^36s$, and $4f^36p$ configurations of Nd III, in which 39 of the 40 previously published energy levels are confirmed and 105 energy levels are experimentally established for the first time. In total, 432 Nd III transitions have been observed in the FT spectra with uncertainties down to a few 10^{-3} cm^{-1}. We also aim to provide insight into how accurate and extensive lanthanide atomic data can be obtained using existing spectroscopic techniques; the analysis of the Nd Penning discharge lamp FT spectra was substantially aided by FT spectroscopy of a Nd hollow cathode discharge, grating spectroscopy of Nd vacuum sliding sparks and Nd-rich stars, consideration of Nd energy level isotope shifts, and calculations using the Cowan code (Cowan 1981; Kramida 2021) parameterised by newly established energy levels.

2. Energy level structure of Nd III

2.1. Background

Nd III belongs to the neutral cerium isoelectronic sequence, with the even-parity ground configuration [Xe] $4f^4$ and lowest-lying singly excited configurations [Xe] $4f^3nl$. Figure 1 shows a schematic diagram of Nd III energy levels of configurations up to nl = 5f, grouped by parent terms of the three 4f electrons under the *LS*-coupling scheme – $4f^3(^ML)nl$. Transitions and levels involving the ground configuration and nl = 5d, 6s, 6p are the focus of this paper. The primary difficulty of investigating Nd III atomic structure had been, and still remains to be, disentangling the immense number of spectral lines, particularly those of the $4f^4$–$4f^35d$ transitions, as the $4f^35d$ configuration is associated with hundreds of energy levels. In the visible-UV spectral region of the Nd discharge lamps, the $4f^4$–$4f^35d$ lines of Nd III also overlap with the complex spectra of Nd I and Nd II due to the low ionisation potentials of these two species. In most cases, empirical atomic structure investigations of the lanthanides require more extensive experimental methodology and data, and more labour-intensive spectral analyses, compared to those of the lighter and less complex atoms with open l = s, p, d subshells.

The first experimental investigations of Nd III atomic structure were carried out by Dieke et al. (1961) and Dieke & Crosswhite (1963) using grating spectroscopy of spark discharges. This led to an unpublished establishment of 29 levels by H. M. Crosswhite, she had provided them for the Martin et al. (1978) compilation and they are found in the Atomic Spectra Database of the National Institute of Standards and Technology (NIST ASD; Kramida et al. 2022). The 29 levels account for classified transitions from 24 levels of $4f^35d$ to all 5 levels of the ground term $4f^4(^5I)$, which were likely deduced from isolating Nd III lines by comparing spectra of discharges at various temperatures (Dieke et al. 1961). H. M. Crosswhite's unpublished lists of 314 classified Nd III lines and 643 lines identified as belonging to Nd III also circulate within the astrophysical community, and the latter proved useful for the present work. Ryabchikova et al. (2006) later proposed revisions for 13 of the 29 levels and classifications for 11 brand new levels of the $4f^35d$ configuration, based on stellar spectroscopy, parameterised Cowan code calculations and Fourier transform spectroscopy of Nd hollow cathode discharges by Aldenius (2001).

2.2. Energy level calculations

Theoretical calculations of atomic structure and transition probabilities are invaluable in experimental establishment of energy levels and classifying observed spectral lines. Bord (2000), Zhang et al. (2002), and Dzuba et al. (2003) published the first theoretical investigations of the Nd III spectrum, all utilising the Cowan code (Cowan 1981). Eigenvector compositions of the $4f^35d$ levels below 33 000 cm^{-1} were published by Zhang et al. (2002) and Ryabchikova et al. (2006) under the *LS*-coupling

scheme. Gaigalas et al. (2019) and Silva et al. (2022) published calculations for many more higher-lying levels and configurations, and the readily available online data from Gaigalas et al. (2019) for level energies, leading *LS* term labels, and transition probabilities proved useful during the initial stages of the present empirical spectrum analysis of Nd III.

More accurate calculations of level energies, eigenvector compositions, and transition probabilities were required in the search for experimentally unknown levels of Nd III in the present work. The Cowan code (Cowan 1981; Kramida 2021) was found suitable for this purpose. The configuration interaction space consisted of the even parity configurations $4f^4 + 4f^25d^2 + 4f^36p + 4f^35f$ and the odd parity configurations $4f^35d + 4f^36s + 4f^37s + 4f^36d + 4f^25d6p$. Initially, the Cowan code calculations were performed in the ab initio pseudo-relativistic Hartree–Fock (HFR) approximation with scaling factors of the Slater and configuration interaction parameters set at 0.85 and 0.70, respectively. The average energies were adjusted so that the energy of the ground level $4f^4\ {}^5I_4$ is zero. To account for the incomplete interaction space, the Slater parameters and additional energy parameters α, β, and γ were then adjusted based on similar calculations of Nd III from Ryabchikova et al. (2006) and on calculations of the neighbouring spectra of Pr II (Mashonkina et al. 2009), Pr III (Palmeri et al. 2000; Wyart et al. 2010, unpublished calculations), Nd II (Wyart 2010; Wyart et al. 2010, unpublished calculations), and Nd IV (Wyart et al. 2007). The energy parameters were adjusted in an iterative process by fitting newly established experimental energy levels when they became available during the empirical spectrum analysis.

The final energy parameters calculated for the $4f^4$, $4f^35d$, $4f^36s$, and $4f^36p$ configurations are listed in Table 1, remaining parameters are available at the CDS. The number of experimental levels was insufficient to fit all energy parameters; α, β, and γ were fixed at their estimated values for all configurations to allow the maximum number of Slater parameters to be fitted. There were enough core terms for all three $F^{2,4,6}$(4f,4f) electrostatic parameters only for the $4f^35d$ configuration. It was possible to fit the levels of the $4f^4$, $4f^36p$ and $4f^35f$ configurations with free F^2(4f,4f) and F^4(4f,4f) parameters when F^6(4f,4f) was fixed at the 0.852 ratio (Fitted/HFR) obtained from the fit of the $4f^35d$ configuration. Only one core term (^{4}I) was available for the $4f^36s$, $4f^37s$, and $4f^36d$ configurations; $F^{2,4,6}$(4f,4f) parameters of these configurations, and of the doubly excited configurations $4f^25d^2$ and $4f^25d6p$, were fixed at their ratios obtained from the fit of the $4f^35d$ configuration.

Level energies of the $4f^25d^2$ and $4f^25d6p$ configurations overlap greatly with other configurations. Corresponding configuration interactions may affect calculated level energies and transition probabilities, especially in cases of close proximity of levels of the same symmetry. Regrettably, no levels were established in these doubly excited configurations, and their energy parameters were adjusted only using information from neighbouring ion spectra and the other Nd III configurations. We note that the estimated energies of the lowest $^5L_6$ levels in the $4f^25d^2$ and $4f^25d6p$ configurations, 72 827 and 126 176 cm^{-1} respectively, are in agreement with those predicted by Brewer (1971) at 72 000 ± 2000 and 126 000 ± 4000 cm^{-1}.

Configurations with the excitation of an electron from the full core subshell $5p^6$ can also influence the calculated atomic structure. Important interactions in the even set are $5p^64f^4 \leftrightarrow 5p^54f^5$ and $5p^64f^36p \leftrightarrow 5p^54f^46p$, those in the odd set are $5p^64f^35d \leftrightarrow 5p^54f^45d$ and $5p^64f^36s \leftrightarrow 5p^54f^46s$. The lowest levels of these 5p-excited configurations are estimated to be situated above 170 000 cm^{-1} and 140 000 cm^{-1}, respectively, in the even and

Table 1. Parameters of the least-squares fit of energy levels of the $4f^4$, $4f^35d$, $4f^36s$, and $4f^36p$ configurations of Nd III in Cowan's codes (extract).

Conf.	Param.	LSF [a] (cm^{-1})	G [b]	HFR [a] (cm^{-1})	Ratio [a,c]
$4f^4$	E_{av}	32 348(22)		35 503	–3156
	F^2(4f,4f)	71 335(105)		92 636	0.770
	F^4(4f,4f)	40 755(201)		57 680	0.707
	F^6(4f,4f)	35 267(f)	3	41 372	0.852
	α(4f)	8(f)		0	
	β(4f)	–310(f)		0	
	γ(4f)	1110(f)		0	
	ζ(4f)	782(4)		849	0.921
$4f^35d$	E_{av}	44 999(43)		36 770	8229
	F^2(4f,4f)	78 070(397)	1	101 378	0.770
	F^4(4f,4f)	49 616(383)	2	63 552	0.781
	F^6(4f,4f)	38 949(554)	3	45 705	0.852
	α(4f)	22(f)		0	
	β(4f)	–600(f)		0	
	γ(4f)	1450(f)		0	
	ζ(4f)	882(2)	4	947	0.932
	ζ(5d)	785(7)		831	0.945
	F^1(4f,5d)	953(81)		0	
	F^2(4f,5d)	19 310(119)		26 408	0.731
	F^3(4f,5d)	0(f)		0	
	F^4(4f,5d)	13 958(275)		13 022	1.072
	G^1(4f,5d)	9138(39)		12 824	0.713
	G^2(4f,5d)	1689(198)		0	
	G^3(4f,5d)	9205(142)		10 202	0.902
	G^4(4f,5d)	0(f)		0	
	G^5(4f,5d)	5148(126)		7735	0.666
$4f^36s$	E_{av}	55 647(49)		47 956	7691
	F^2(4f,4f)	78 723(400)	1	102 226	0.770
	F^4(4f,4f)	50 064(387)	2	64 126	0.781
	F^6(4f,4f)	39 310(559)	3	46 129	0.852
	α(4f)	22(f)		0	
	β(4f)	–600(f)		0	
	γ(4f)	1450(f)		0	
	ζ(4f)	886(2)	4	953	0.932
	G^3(4f,6s)	2393(72)		2870	0.834
$4f^36p$	E_{av}	88 343(29)		79 811	8544
	F^2(4f,4f)	78 655(146)		102 329	0.769
	F^4(4f,4f)	49 923(164)		64 196	0.778
	F^6(4f,4f)	39 344(f)	3	46 180	0.852
	α(4f)	22(f)		0	
	β(4f)	–600(f)		0	
	γ(4f)	1450(f)		0	
	ζ(4f)	888(2)		954	0.930
	ζ(6p)	2467(10)		1989	1.240
	F^1(4f,6p)	739(45)		0	
	F^2(4f,6p)	6396(359)		7861	0.814
	G^2(4f,6p)	2082(55)		1981	1.051
	G^3(4f,6p)	0(f)		0	
	G^4(4f,6p)	1490(93)		1791	0.832

Notes. The full version of this table is available at the CDS. [a]Parameter values determined in the ab initio pseudo-relativistic Hartree–Fock (HFR) and least-squares-fitted (LSF) calculations and their ratio. Standard deviations of the fitted LSF parameters are in parentheses, where 'f' means the parameter was fixed. [b]Parameters in each numbered group (G) were linked together by sharing the same ratios to their corresponding HFR values. [c]Differences between LSF and HFR parameters are given for E_{av}.

Table 2. Nd–Ar PDL FT spectra parameters.

Spec. (1)	Spec. range (cm^{-1}) (2)	Res. (cm^{-1}) (3)	Pressure (10^{-3} mbar) (4)	Current (mA) (5)	No. of co-adds (6)	Photomult. tube (7)	Optical filter (8)	Int. calib. lamp (9)	k_{eff} (10^{-7}) (10)
A	11 890–17 687	0.045	1.7	750	8	R928	OG530	W	1.74 ± 0.14
B	17 687–21 300	0.050	2.2	750	7	R11586	GG475	W	1.39 ± 0.09
C	21 300–25 369	0.050	2.3	650–750	19	R11586	GG385+SP500	W	−3.10 ± 0.20
D	25 369–32 480	0.055	2.4	750	21	R11586	UG5-C	W	−2.95 ± 0.12
E	32 480–44 422	0.070	1.7	750	23	R7154	–	D_2	−2.88 ± 0.19
F	44 422–53 822	0.080	2.0	750	32	R8486	180-B-1D	D_2	4.32 ± 0.38

Notes. Column 1 is the spectrum name, Col. 2 is the spectral range within which the corresponding transitions were measured, Cols. 3–5 are the spectral resolution, running pressures and currents, respectively, Col. 6 is the number of interferogram co-adds, and Cols. 7–9 are the detector, filter, and intensity calibration lamp used, respectively, W indicates tungsten lamp and D_2 indicates deuterium lamp. The final column lists the wavenumber calibration factors and their uncertainties.

odd systems, and thus lie far above the levels found in this work. Therefore, configuration interactions with the 5p-excited configurations are not expected to significantly influence the calculated branching ratios used to experimentally find the levels that are far below the 5p-excited configurations. Direct inclusion of the 5p-excited configurations in the configuration interactions led to very large matrix dimensions, beyond the limits of the available computational resources initially aimed at experimental spectra analysis. Therefore, the influence of 5p-excited configurations was taken into account indirectly by variations of Slater and spin–orbit parameters as well as using some of Slater parameters of illegal ranks.

Using the energy and configuration interaction parameters from Table 1, the standard deviations of the predicted level energies from their experimental values were 29 and 36 cm^{-1} for the even and odd level systems, respectively. Corresponding eigenvector compositions and transition probabilities were also calculated. In searching for experimentally unknown energy levels, these calculations addressed the insufficient accuracy in the theoretical predictions by Gaigalas et al. (2019), particularly for higher-lying energy levels at higher level densities.

2.3. Accuracy of calculated transition probabilities

Branching ratios and transition probabilities calculated using the Cowan code were one of the main tools for line classification, through their comparison with experimental relative line intensities. Since the experiments were not designed to measure branching ratios, the uncertainty of calculated branching ratios cannot be inferred from experimental values and so the calculated branching ratios should only be considered as guides. The calculated branching ratio uncertainties are expected to be no smaller than, but comparable to the uncertainties of the measured relative intensities within the FT spectra, and are expected to increase with increasing level mixing and nearby level density, and decreasing absolute transition probability.

Potential offsets in the calculated lifetimes and absolute transition probabilities are expected but are of negligible concern for the classification of Nd III transitions in the present work. For context, the five experimental lifetimes of Zhang et al. (2002) are on average 40% greater compared to the present calculations and the calculated transition probabilities of Gaigalas et al. (2019) are on average estimated to be three times smaller in the present calculations. Furthermore, ignoring core-excitation configurations may also contribute to overall shifts in lifetimes (see Sect. 6).

3. Experimental details

3.1. FT spectroscopy of the Nd Penning discharge lamp

All level energies within this publication were determined using spectral lines measured by the high-resolution $f/25$ Imperial College VUV FT spectrometer (Thorne et al. 1987), using a custom-built water-cooled Penning discharge lamp (PDL), designed by Heise et al. (1994), with 99.5% pure Nd cathodes at natural isotopic abundances, a magnesium fluoride window, and argon as the sputtering carrier gas. The 0.5% impurities in the cathodes were primarily iron and praseodymium, the strongest transitions of Pr I–III could not be reliably identified due to high photon noise in the visible region. Stable lamp running pressures and currents were chosen such that the signal-to-noise ratios (S/Ns) of the previously classified known Nd III transitions were maximised, which were (1.7–2.4) × 10^{-3} mbar and 650–750 mA, respectively. The discharge remained stable for 2–3 h under these conditions before the Nd cathodes were depleted. The PDL was chosen as the light source for its lower-pressure and higher-temperature stable discharge with higher Nd III populations compared to those produced by the alternative hollow cathode discharge lamps commonly used in FT spectroscopy. As far as we know, no records on producing Nd spectra using a PDL light source have been published previously.

Nd–Ar PDL FT spectra were recorded in six separate spectral regions within 11 500–54 000 cm^{-1} (8695–1852 Å), their experimental details are summarised in Table 2. Spectral ranges spanning the visible were narrower (in cm^{-1}) compared to the UV regions, this was to reveal weaker lines by reducing photon noise from the intense and numerous Nd I-III lines in the visible. Spectral resolving power was limited by predominantly the Doppler line widths as no instrumental ringing was observed. Observed spectral lines from all six spectra were fitted to create a line list used in the energy level search. Most lines were fitted using the Voigt profile, where the Lorentzian components of the line widths were observed around one order of magnitude smaller than the Gaussian (Doppler) components. The statistical uncertainty in the wavenumber σ_{obs} of a spectral line estimated by Voigt profile fitting is (Brault 1987; Davis et al. 2001)

$$\Delta\sigma_{obs} \approx \frac{1}{\sqrt{N}} \frac{FWHM}{S/N}, \quad (1)$$

where N is the number of points within the full width at half maximum (FWHM), and S/N was capped at 100 to prevent unrealistically low uncertainties. Details regarding non-Voigt profile

spectral line fitting will be discussed in Sect. 4.3. The noise level of each spectrum was an average of three estimates of the root-mean-squared noise evenly across its spectral range, taken from regions with relatively fewer lines. The noise level was found to be invariant with wavenumber for spectra E and F but varied by up to 20% for spectra A and C and by up to 40% for spectra B and D. These variations are attributable to the high line-densities below 30 000 cm^{-1} (above 333 nm), where weak lines were inseparable from noise in the noise level calculation. Therefore, S/Ns and statistical wavenumber uncertainties of spectral lines in spectra A, B, C, and D are less reliable compared to those of spectra E and F. This limitation did not hinder the analysis of Nd III atomic structure since the observed wavenumbers of all classified unblended Nd III lines agree with their Ritz values[1] within standard uncertainties. Furthermore, most level energies were predominantly weighted in the level optimisation using lines with S/N above the 100 cap and/or lines within spectra E and F with the most reliable wavenumber uncertainties.

The final column of Table 2 lists wavenumber calibration factors $k_{\rm eff}$ of observed wavenumbers $\sigma_{\rm obs}$ in each spectrum, where the calibrated wavenumbers $\sigma_{\rm cal}$ are defined by (Haris & Kramida 2017):

$$\sigma_{\rm cal} = (1 + k_{\rm eff})\sigma_{\rm obs}. \tag{2}$$

This calibration factor mainly accounts for the finite aperture size of the FT spectrometer and any misalignment of the lamp and the spectrometer's calibration laser (Learner & Thorne 1988). Wavenumber calibration was carried out using 13 of the 28 Ar II reference lines recommended by Learner & Thorne (1988) within spectrum C, using their corresponding reference wavenumbers measured by Whaling et al. (1995). The remaining Ar II reference lines in spectrum C were unsuitable due to low S/N and/or blending with Nd lines.

A calibration factor $k_{{\rm eff},i}$ was determined for each reference wavenumber $\sigma_{{\rm cal},i}$ in a spectrum using its observed wavenumber in Eq. (2), and then the $k_{\rm eff}$ of the spectrum was the weighted average

$$k_{\rm eff} = \frac{\sum_i w_i\, k_{{\rm eff},i}}{\sum_i w_i}, \tag{3}$$

with weights $w_i = (\Delta k_{{\rm eff},i})^{-2}$, where the $\Delta k_{{\rm eff},i}$ were the absolute uncertainties of $k_{{\rm eff},i}$ determined by Eq. (2). The uncertainty in the calibration factor $k_{\rm eff}$ was given by (Radziemski & Andrew 1965; Haris & Kramida 2017)

$$\Delta k_{\rm eff} = \frac{\sqrt{\sum_i [w_i + w_i^2 (k_{\rm eff} - k_{{\rm eff},i})^2]}}{\sum_i w_i}. \tag{4}$$

The systematic uncertainties $\Delta\sigma_{\rm sys}$ in wavenumber calibration are given by $\sigma_{\rm obs}\Delta k_{\rm eff}$, which were added in quadrature with $\Delta\sigma_{\rm obs}$ from Eq. (1) to yield the final wavenumber uncertainty for each line.

The above was repeated for each of the other spectra by using calibrated lines within overlapping spectral regions as wavenumber references. These were selected from lines that were non-blended, at intermediate S/N, and with no evidence of self-absorption in their fit residuals. In this procedure, the $\Delta\sigma_{\rm sys}$ of each other spectrum could become lower than that of spectrum C, for example, due to low RMS residuals of $k_{{\rm eff},i}$, higher S/Ns, and/or a larger number of reference lines i. This was addressed by conservatively estimating the systematic uncertainty of a spectrum to be a linear sum including all correlated systematic uncertainties, for example, the systematic uncertainty of spectrum F was

$$\Delta\sigma^{\rm F}_{\rm sys} + \Delta\sigma^{\rm E}_{\rm sys} + \Delta\sigma^{\rm D}_{\rm sys} + \Delta\sigma^{\rm C}_{\rm sys}, \tag{5}$$

where the values from previous spectra were from overlapping spectral regions. This procedure was later verified by the lack of any systematic offsets seen between the observed and Ritz wavenumbers of transitions from energy levels with transitions across multiple spectra. Differences between observed and Ritz wavenumbers of all lines included in the level optimisation procedure are within 1.2 times the estimated final wavenumber uncertainties, which do not exceed ±0.003 cm^{-1} (±0.0003 Å at 3000 Å) for unblended lines with $S/N > 100$ and no features of self-absorption.

Relative intensities (areas under the lines) measured in the FT spectra correspond to relative photon fluxes, which are conveniently comparable to the ratios of theoretical weighted transition probabilities during line classification after calibration. All six Nd–Ar PDL FT spectra were intensity calibrated using either a tungsten standard lamp (IR to UV) or a deuterium standard lamp (UV to VUV). Intensities measured in different spectral regions were placed onto a common relative intensity scale set by spectrum C, using lines within overlapping regions of neighbouring spectra. When possible, only known Nd III lines were used. The calibrated relative intensities are only recommended as a rough guide as the experiments were not designed for branching ratio measurements. As a guide, a minimum uncertainty of 15% is recommended for relative intensities of the highest S/N transitions to the ground term, and much higher uncertainties are expected for low S/N lines and when comparing intensities between the different spectral regions listed in Table 2 predominantly due to different lamp conditions. Nevertheless, this accuracy in line intensities was sufficient for the empirical Nd III atomic structure analysis of this work.

3.2. FT spectroscopy of the Nd hollow cathode lamp

Spectra of a custom-built water-cooled hollow cathode discharge lamp (HCL) with a 99.5% pure Nd cathode (natural isotope abundances) were also recorded using Ar carrier gas, with similar numbers of co-adds and the identical six spectral ranges, detectors, filters, and intensity calibration lamps listed in Table 2, but at higher resolutions due to the narrower Doppler line widths of the HCL spectral lines. Stable conditions were chosen to maximise the S/Ns of previously classified Nd III transitions at 0.43 mbar and 450 mA running pressure and current, respectively. Under these conditions, the HCL ran stably for experiments over many weeks of use until cathode depletion.

The HCL spectra provided useful information on line intensities and better-resolved line profiles from a Nd–Ar plasma at a lower effective temperature compared to that of the PDL. The FWHM of symmetrical lines showing negligible broadening from isotope/hyperfine structure and self-absorption within the PDL spectra were around 1.5 times larger compared to those within the HCL, so the statistical wavenumber uncertainties from Eq. (1) of the highest S/N HCL lines were generally lower in comparison. However, all Nd III lines in the HCL spectra were lower in S/N and many were absent compared to the PDL spectra. Except for the few highest S/N Nd III lines in the visible, there were no improvements in wavenumber uncertainties from using lines in the HCL

[1] Ritz wavenumbers are the differences between level energies optimised using all observed wavenumbers, see Sect. 5.1.1 for more details.

Table 3. Nd vacuum sliding spark grating photographic plates and their spectral ranges used.

Spec. no.	Date; no. [a]	Instrument [b]	Spec. range [c] (Å)
1	November 10 2002	ISAN-NIVS 6.65 m	390–1525
2	November 28 2002	ISAN-NIVS 6.65 m	1904–2327
3	No. 514a Track no. 1	NIST-NIVS 10 m	2333–2570
4	No. 522a, b Track no. 5	NIST-NIVS 10 m	2651–3213

Notes. [a]No. is the serial plate number according to the NIST archive classification. [b]ISAN – The Insititute of Spectroscopy of the Russian Academy of Sciences, Troitsk, Russia; NIST – National Institute of Science and Technology, Gaithersburg, USA; NIVS – normal incidence spectrograph. [c]Indication of which plates the classified lines of Table 7 belong to. In the present work, spectrum no. 1 was used to check possible blends by lines of the second diffraction orders.

spectra. Moreover, instrumental ringing was observed for narrower FWHM lines in the visible-IR regions of the HCL spectra at the highest available resolution (0.037 cm^{-1}) of the Imperial College VUV spectrometer. Therefore, line identification and wavenumber fitting using the under-resolved HCL spectral lines was less reliable and the HCL spectra were not used for wavenumber measurements.

3.3. Grating spectroscopy of Nd vacuum sliding sparks

Two sets of Nd vacuum sliding spark (VS) spectra of currents up to 1500 A were used for the analysis of Nd III atomic structure. The spectra in the 390–1525 Å and 1600–2536 Å ranges were taken on the 6.65 m normal incidence spectrometer at the Institute of Spectroscopy in Troitsk, Russia. The spectrometer is equipped with a 1200 lines mm^{-1} grating providing a 1.25 Å mm^{-1} plate factor. The spectra were recorded on Ilford Q photographic plates and measured on the automatic comparator with a scanning step of 0.3 µm controlled by the system for automatic processing of photo-spectrograms designed by Azarov (1991). The other set of spectra consists of photographic plates recorded on the 10 m normal incidence spectrograph at NIST. These plates covered the range 2330–2619 Å and 2547–3250 Å and were scanned by an Epson Expression 1000 XL scanner, the spectral line positions and intensities were measured using the GFit code (Engström 1998). A summary of the Nd VS grating spectra is given in Table 3.

Impurity lines of oxygen, carbon, nitrogen, and silicon in various ionisation stages (Kramida et al. 2022), as well as lines of Nd IV (Wyart et al. 2007) and Nd V (Meftah et al. 2008), were used for wavelength calibration initially. After the measurement and classification of Nd III lines by FT spectroscopy in this work, the Nd VS grating spectra were calibrated again with the addition of the Nd III Ritz wavelengths. The final uncertainties of unblended and symmetric lines of moderate intensity were estimated at ±0.006 Å.

In contrast to the Nd–Ar HCL FT spectra, the Nd VS grating spectra were a guide for relative line intensities at higher effective temperatures compared to the PDL. Furthermore, these grating spectra also contained weaker Nd III lines that were absent in the Nd–Ar PDL FT spectra. The Nd VS grating spectra 2, 3, and 4 of Table 3 were intensity calibrated onto a common relative scale using classified Nd III lines within overlapping regions. The measured line blackening was transformed to intensity using approximate wavelength-independent model response curves and energy flux sensitivities of the photographic plates, which were placed onto a linear relative scale approximately corresponding to the weighted transition probabilities calculated during this work. In principle, the transition probabilities should be weighted with wavenumber when comparing with the measured relative energy fluxes. However, for transitions of an energy level observed in the Nd VS grating spectra, the differences in relative intensities introduced by the wavenumber weighting are much smaller than the relative intensity uncertainties from calibration; the intensities should only be considered qualitative due to uncertainties in the response curves of the grating spectrometers and the non-linearity of the photographic plate response curves and sensitivities.

3.4. Stellar spectroscopy of Nd

The laboratory analysis of the Nd III spectrum was also supplemented by the analysis of high-resolution, high S/N spectra of magnetic chemically peculiar Ap stars with large atmospheric Nd overabundance. Two tepid stars of similar atmospheric parameters (effective temperature and surface gravity) but different surface magnetic fields were chosen: HD 170973 with $T_{\rm eff} = 11\,200$ K, $\log g = 3.8$ (Ryabchikova et al. 2011) and HD 144897 with $T_{\rm eff} = 11\,250$ K, $\log g = 4.0$ (Ryabchikova et al. 2006). The spectra of both stars ranged from 3030 to 10 400 Å and were recorded at resolving power $R = 80\,000$ by the UVES instrument at the ESO VLT under the programme 68.D-0254. More details of the observations and spectrum reduction are given in Ryabchikova et al. (2008). The surface magnetic field $\langle B_s \rangle = 8.8$ kG in HD 144897 was estimated from Zeeman splitting of spectral lines (Ryabchikova et al. 2006), while the absence of any splitting in spectrum of HD 170973 together with one estimate of the longitudinal magnetic field $\langle B_z \rangle = 392 \pm 5$ G (G. Wade, priv. comm.) did not indicate the presence of a surface magnetic field stronger than 1 kG in the atmosphere of HD 170973. Both stars rotate slowly with projected rotational velocity $v_e \sin i = 8.5$ km s^{-1} (HD 170973) and $v_e \sin i$=3 km s^{-1} (HD 144897), where v_e is the equatorial rotation velocity of the star and i is the angle between the rotational axis and line of sight.

The atmospheres of the two stars are very rich in rare-earth elements, their average Nd abundances[2] exceed the solar value by four orders of magnitude. In the solar photosphere, $\log \varepsilon_{\rm Nd} = 1.42$ (Lodders 2021), whereas $\log \varepsilon_{\rm Nd} = 5.39 \pm 0.18$ for HD 170973 (Kato 2003). In the present work, the reference Nd abundance of HD 170973 was recalculated at 5.63 ± 0.14 using $T_{\rm eff} = 11\,200$ K, $\log g = 3.8$ (Ryabchikova et al. 2011), and equivalent widths of 30 Nd III lines previously classified by Ryabchikova et al. (2006) and observed in the Nd–Ar PDL FT spectra. The reference abundance for HD 144897 was estimated at $\log \varepsilon_{\rm Nd} = 5.59 \pm 0.20$ (Ryabchikova et al. 2006). The temperatures, high Nd abundances, and differing surface magnetic field strengths of the two stars favoured the careful analysis of Nd III lines in their spectra.

[2] Nd abundance is expressed as $\log \varepsilon_{\rm Nd} = \log(N_{\rm Nd}/N_{\rm tot}) + 12.04$, where $N_{\rm Nd}$ and $N_{\rm tot}$ are number densities of neodymium and total number of atoms, respectively.

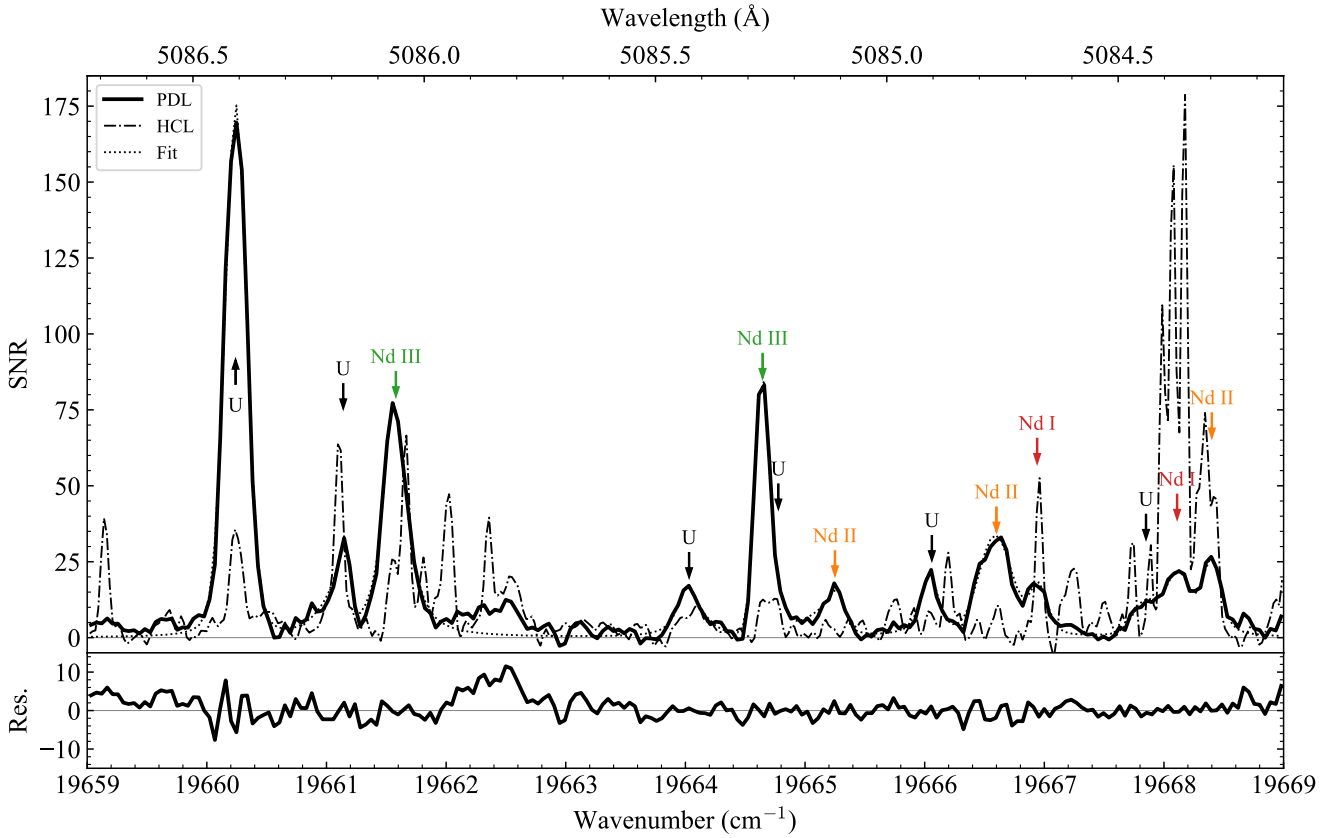

Fig. 2. Emission spectra of Nd recorded using Fourier transform spectroscopy between 19 659 and 19 669 cm^{-1} (vacuum) containing lines with intermediate S/Ns and showing weak and uncertain blended spectral lines. Penning discharge lamp (PDL) and hollow cathode lamp (HCL) spectra are the solid and dash-dotted lines, respectively. The dotted line shows fits to the 13 lines identified in the PDL spectrum, residuals are shown at the bottom. Lines identified and fitted in the PDL spectrum are indicated by vertical arrows and labels, those with label U are unclassified.

4. Spectrum of the Nd Penning discharge lamp

4.1. Spectrum and line identification

A total of 21 584 line wavenumbers were fitted in the Nd–Ar PDL FT spectra using the peak-finding algorithm of Nave et al. (2015) and by manual selection. The line list contained transitions of Nd I–IV, Ar I–III, and Fe I–II (Nd cathode impurity), the numbers of observed known lines of each species are listed in Table 4. Apart from Nd III, the number of classified lines of each other species is uncertain due to the large quantity of unidentified blended and weak lines, as well as coincidental wavenumber matches within uncertainties. For Nd I and Nd II, a significant number of matches with Ritz wavenumbers are expected to be coincidental and incorrect. Moreover, many Nd I-II levels from the NIST database are also uncertain with only configuration and J value assignments. Figure 2 highlights the difficulties and uncertainties of line fitting with a 10 cm^{-1} section of the Nd FT spectrum, measured in both the PDL and HCL and representative of the most line-rich and intense regions 15 000–30 000 cm^{-1} (6666–3333 Å), where a large fraction of the Nd III $4f^4$–$4f^3$5d, Nd I, and Nd II transitions lie.

Weak lines and weak blends, such as the feature observed at 19 662.5 cm^{-1} of the PDL spectrum in Fig. 2, were extremely common and often missed by the peak finding algorithm and manual fine-tuning when fitting line profiles for the line list. The labour cost of analysing and fitting every single line around the noise level was considered not feasible due to their ubiquity and large uncertainties from high susceptibility to blending. For example, in the comparison between the PDL and HCL spectra of Fig. 2, all 13 PDL lines of the 10 cm^{-1} section were arguably blended to some extent. The incompleteness and inaccuracy of the list of observed wavenumbers were two of the most limiting

Table 4. Species observed and the numbers of lines fitted in Nd–Ar PDL FT spectra.

Species	No. of lines [a]	Line list for identification
Nd I	1636	NIST ASD [b]
Nd II	6574	NIST ASD [b]
Nd III	579	This work [c]
Nd IV	54	Wyart et al. (2007)
Ar I	48	Whaling et al. (2002)
Ar II	430	Saloman (2010)
Ar III	90	Saloman (2010)
Fe I	468	Nave et al. (1994)
Fe II	294	Nave & Johansson (2012)
Unclassified	11 411	N/A [d]

Notes. [a]Number of lines whose wavenumbers matched previously observed wavenumbers within ±0.2 cm^{-1} for Nd IV, and ±0.05 cm^{-1} for the other species. [b]Using Ritz wavenumbers allowed by $\Delta J = 0, \pm 1$, but not $J = 0 \leftrightarrow 0$ and parity selection rules for E1 transitions of the energy levels on the NIST ASD (Kramida et al. 2022) that were mostly from Martin et al. (1978); Blaise et al. (1971, 1984). [c]147 of the 579 lines belong to the $4f^3$6p–$4f^3$7s and $4f^3$6p–$4f^3$6d transitions, which will be reported in a future publication. [d]An estimate excluding multiply identified lines, unknown coincidental wavenumber matches, and unfitted lines that are too weak or in unknown blends.

factors in the empirical search for energy levels; expected transitions may be missing in the line list due to weak and unfitted lines or inaccurately fitted blends. Around 2000 of the 21 584 lines were in fact fitted later during the empirical Nd III energy level analysis when more thorough spectrum fitting of blends and weak lines became necessary within spectral regions containing weak Nd III transitions of interest.

The primary assistance in line and blend identification was provided by the HCL spectra, which produced an Nd–Ar discharge at a lower effective temperature with narrower Doppler widths. Lines of Nd I could also be identified with reasonable certainty, as Nd I was the only Nd species with reduced relative intensities in the PDL compared to that of the HCL, and this is noticeable in Fig. 2. Self-absorption was observed in the PDL for a fraction of Nd II transitions between the lowest-lying levels, evident from the self-reversals, flattened tops, or most commonly the reversed 'W' Voigt profile fit residuals of these line profiles. The line in Fig. 2 at 19 660.2 cm $^{-1}$ was unclassified but showed features of self-absorption, indicating the possibility of it being an unclassified Nd II transition.

Compared to the line-rich visible-UV regions, the Nd–Ar PDL spectrum was relatively much less intense in the deeper UV (30 000–50 000 cm^{-1}, 3333–2000 Å) and was not plagued by a large number of blended and weak lines. This indicated lower populations of Nd III ions at the 4f^{3}6p, 4f^{3}7s, 4f^{3}6d and doubly excited configurations, and of Nd IV ions at the 4f^{2}5d and 4f^{2}6p configurations; their transitions to lower levels were expected in this region but were observed at low S/Ns. The lines with the highest intensities in this region were the 4f^4 ^{5}I–4f^3(^{4}G°)5d transitions of Nd III around 35 500 cm^{-1}.

4.2. Nd III isotope shifts

Many Nd lines of the FT spectra showed similar non-Voigt line profiles despite the likelihood of line blending. The cathodes of the PDL and HCL contained natural abundances of the 7 stable isotopes (Berglund & Wieser 2011): ^{142}Nd (27.15%), ^{143}Nd (12.17%), ^{144}Nd (23.80%), ^{145}Nd (8.29%), ^{146}Nd (17.19%), ^{148}Nd (5.76%), and ^{150}Nd (5.64%), all of which have non-negligible abundance. Energy levels of ^{143}Nd and ^{145}Nd also have hyperfine structure. Consideration of isotope shifts of different transition arrays was a key component in the empirical atomic structure analyses of Nd I and Nd II (e.g. Blaise et al. 1971, 1984; Wyart 2010). Likewise, isotope line profiles of the 4f^4–4f^{3}5d Nd III transitions were indispensable for their classifications in this work.

Observations of Nd III isotope structure were first made by Aldenius (2001). Examples observed in the FT spectra of the present work are shown in Fig. 3. The transition 4f^4 ^{5}I$_6$–4f^3(^{4}I°)6s ($\frac{9}{2}$, $\frac{1}{2}$)°$_5$ was the only Nd III line observed in the HCL spectrum with resolved ^{142}Nd, ^{144}Nd, and ^{146}Nd isotope components. The ^{148}Nd and ^{150}Nd components at higher wavenumbers are uncertain due to smaller relative abundances, low S/Ns, and hyperfine structure of the ^{143}Nd and ^{145}Nd isotopes. This pattern is consistent with many isotope profiles observed for Nd I (e.g. 19 668.1 cm^{-1} of Fig. 2) and Nd II (e.g. Fig. 2 of Koczorowski et al. 2005). We note that the wavenumber order of isotope component transitions depends on the isotope shifts of both the upper and lower levels. In heavy atoms such as those of Nd, the field shift is expected to be greater than the mass shift, where perturbations to level energies are positive (electrons become less tightly bound) and increase with increasing overlap between nuclear volume and electron density. In Fig. 3, electron densities of all upper-level configurations are larger around the nucleus compared to those of the lower-level configuration, and so the shifts in transition wavenumber (e.g. relative to ^{142}Nd), are positive and increase in size with increasing nucleon number; the situation is opposite to that of the Nd II transition in Fig. 2 of Koczorowski et al. (2005), where its lower level has higher electron densities around the nucleus.

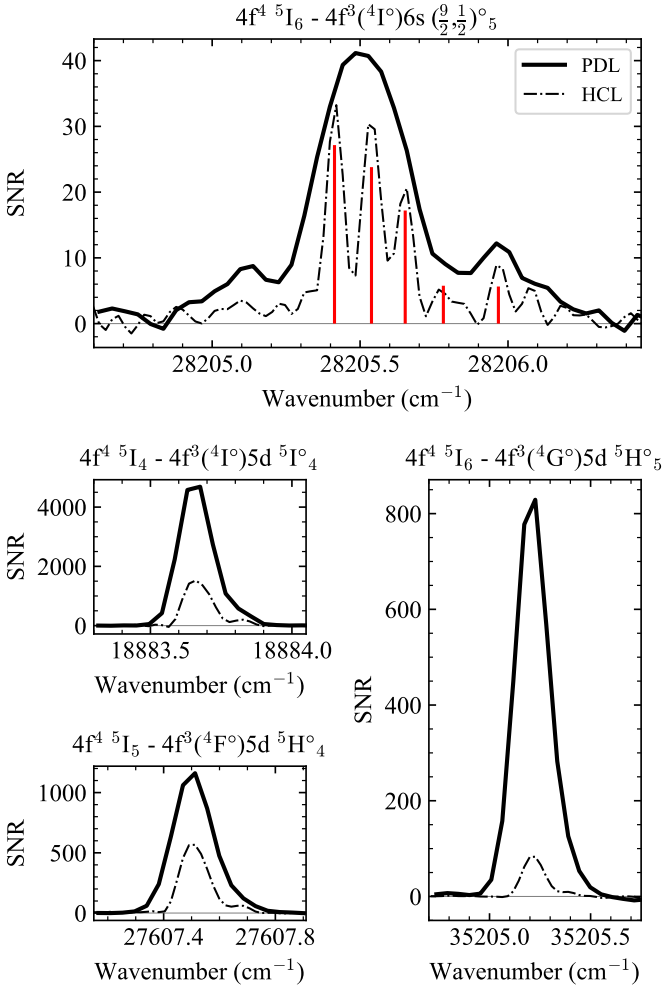

Fig. 3. Isotope shifts of four Nd III lines observed by Fourier transform spectroscopy of the Nd–Ar Penning discharge lamp (PDL, solid) and the Nd–Ar hollow cathode lamp (HCL, dash-dotted line). For 4f^4 ^{5}I$_6$–4f^3(^{4}I°)6s ($\frac{9}{2}$, $\frac{1}{2}$)°$_5$, isotope components of ^{142}Nd, ^{144}Nd, ^{146}Nd, ^{148}Nd, and ^{150}Nd are marked tentatively from left to right with red vertical lines in relative abundance ratios from Berglund & Wieser (2011), remaining features are likely hyperfine structures of ^{143}Nd and ^{145}Nd or blended weak lines.

Isotope shifts added another layer of complexity in line fitting; in Fig. 2, the unclassified line of 19 667.9 cm^{-1} may have been misidentified since in the HCL spectrum it could be a part of the isotope structure of the Nd I line. Almost all classified 4f^4–4f^{3}5d transitions of Nd III showed an unresolved ^{150}Nd right-side wing within the PDL spectra (e.g. see Fig. 3), which was an essential clue to their classification when observed at a sufficient S/N.

4.3. Line profile fitting

Least-squares fitting using the Voigt profile was not suitable for all observed PDL spectral line profiles. Lines showing significant isotope structure were fitted by using the centre-of-gravity (COG) method, where the line wavenumber is an average of

wavenumbers within a manually specified range weighted by S/N. For COG fitted lines, statistical wavenumber uncertainties from Eq. (1) were doubled. However, the unresolved ^{150}Nd right-side wings of the 4f^4–4f^{3}5d Nd III transitions were not always recognisable during visual inspections and manual corrections to the output of the peak-finding algorithm, particularly at intermediate and lower S/Ns. In this case, not only would the isotope shift clue for line classification be lost, but the differences between wavenumbers from Voigt and COG fits were often larger than their statistical uncertainties. This caused even more inaccuracies in the fitted wavenumbers, which obstructed the search for Nd III energy levels. Additionally, COG fitting may not be as accurate for blended and weak lines, as specifying wavenumber limits of such line profiles could range from non-trivial to impossible. While COG wavenumber uncertainties due to losing weak isotope or hyperfine structure components to the noise can be estimated (e.g. Kramida et al. 2017), methods to more reliably identify lines with weak isotope structure and to fit these lines within partially resolved blends were still required.

An asymmetric Voigt profile was used to quantify the unresolved ^{150}Nd right-side wings of the 4f^4–4f^{3}5d transitions, and to more accurately estimate wavenumbers of similarly asymmetric line profiles. The dominant Doppler width of the Voigt profile w was varied as a sigmoid function of wavenumber parameterised by an asymmetry factor a (Stancik & Brauns 2008),

$$w(\sigma) = \frac{2w_0}{1 + e^{a(\sigma-\sigma_0)}}, \tag{6}$$

where w_0 and σ_0 are the Doppler width and wavenumber of the usual Voigt profile ($a = 0$), respectively. The wavenumber of the fitted line was estimated using the COG of this asymmetric Voigt profile. Lines resembling the ^{150}Nd right-side wing asymmetry would have $a < 0$.

By no means was this asymmetric Voigt profile an accurate physical description of isotope shifts, but overall improvements in wavenumber fitting were achieved for the 4f^4–4f^{3}5d transitions. In the example shown in Fig. 4, the choice of COG wavenumber limits was difficult due to slight blending with a second weaker line, the unresolved right wing was not obvious from inspection and only evident from Voigt fit residuals. When fitted using the Voigt profile, the observed wavenumber differed from Ritz and asymmetric Voigt fit values by more than the wavenumber uncertainty. The example in Fig. 4 was fitted with $a = -1.62$. Statistical uncertainties from Eq. (1) were doubled for any lines with $|a| > 1$, and a was fixed at 0 for lines with S/Ns lower than 10.

Compared to using the normal Voigt function, wavenumbers from asymmetric Voigt fits were closer to and within uncertainties of manual COG values. This fitting method also alleviated a prohibitive amount of labour otherwise induced by manually specifying limits of COG wavenumbers of thousands of such lines. Flexible adjustments of the line list using all three line fitting methods were readily available using a custom computer program, where each line of the line list contained the essential parameters: S/N, FWHM, calibrated wavenumber (Voigt or COG) and its final uncertainty, calibrated relative intensity, method of fitting, and the asymmetry factor a.

5. Empirical spectrum analysis of Nd III

Initially, results from previously published experimental investigations of Nd III were used to classify Nd III lines, and then unclassified lines were used in the search for new energy levels using theoretical calculations as a guide. The methodology is discussed in more detail in Sect. 5.2.

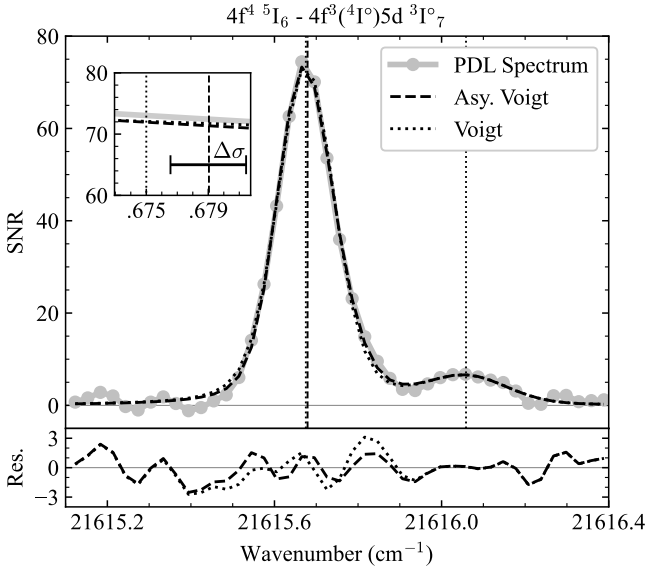

Fig. 4. Nd III transition 4f^4 ^{5}I$_6$–4f^3(^{4}I°)5d ^{3}I°$_7$ at 21 615.679 cm^{-1}, slightly blended with an unclassified line at 21 616.058 cm^{-1}. Fits using asymmetric Voigt and normal Voigt profiles are shown in dashed and dotted lines, respectively, their residuals are shown in the lower plot and their fitted wavenumbers are shown by the vertical lines. The wavenumber uncertainty of the asymmetric Voigt fit $\Delta\sigma$ is shown in the zoomed section.

5.1. Results

5.1.1. Energy levels

Wavenumbers of the 579 classified Nd III transitions from the Nd–Ar PDL FT spectra were input into the LOPT program (Kramida 2011) to estimate the optimum level energies and Ritz wavenumbers by minimisation of the squared difference between observed wavenumbers and their Ritz values, weighted by inverse squares of the observed wavenumber uncertainties. The input wavenumbers were separated into groups corresponding to each of the six spectra listed in Table 2 to estimate possible systematic shifts in wavenumbers due to uncertainties in wavenumber calibration. The uncertainty of a level energy was estimated by adding its uncertainty relative to the ground level and its estimated systematic shifts from each spectrum in quadrature (Kramida 2011).

The experimentally established energy levels of the 4f^4, 4f^{3}5d, 4f^{3}6s, and 4f^{3}6p configurations of Nd III from this work are listed in Table 5 in order of ascending energy of their assigned configurations and terms. Only the lowest-lying terms of each configuration are presented, the full table is available at the CDS. Pure *LS*-coupling basis functions were used to label energy levels of the 4f^4, 4f^{3}5d and 4f^{3}6p configurations. Under this scheme, purity is high overall for the lowest-lying terms of the 4f^4 and 4^{3}5d configurations. Higher-lying levels of these two configurations, and the 4f^{3}6p levels, were mixed; violation of the *LS*-coupling selection rules (i.e. $\Delta S = 0$ and $\Delta L = 0, \pm 1$ but not $L = 0 \leftrightarrow 0$) was thus very common. For the 4f^3(^{4}I°)6s levels, *jj*-coupling of the 6s electron with the 4f^3(^{4}I°) core was used for assignment as the basis functions under this coupling scheme better represented their assigned levels.

Table 5. Energy levels experimentally established for the $4f^4$, $4f^3 5d$, $4f^3 6s$, and $4f^3 6p$ configurations of Nd III (extract).

Assignment Conf.	Term	J	Energy (cm^{-1})	N	ΔE_1 (cm^{-1})	ΔE_2 (cm^{-1})	g	Eigenvector composition (%)		
$4f^4$	^{5}I	4	0.000(0)	22(5)	–8	0	0.604	97 $4f^4$ ^{5}I	1 $4f^4$ ^{3}H4	1 $4f^4$ ^{3}H3
		5	1137.794(2)	31(7)	–3	65	0.901	98 $4f^4$ ^{5}I	1 $4f^4$ ^{3}H4	
		6	2387.544(2)	34(7)	–4	124	1.071	99 $4f^4$ ^{5}I		
		7	3714.548(2)	29(6)	–12	172	1.177	98 $4f^4$ ^{5}I	1 $4f^4$ ^{3}K2	
		8	5093.257(3)	17(4)	–23	209	1.247	96 $4f^4$ ^{5}I	2 $4f^4$ ^{3}K2	1 $4f^4$ ^{3}K1
		⋮	⋮	⋮	⋮	⋮	⋮	⋮	⋮	⋮
$4f^3(^4I°)5d$	^{5}L°	6	15 158.154(7)	2(0)	–52	–100	0.724	93 (^{4}I°)5d ^{5}L°	3 (^{2}H2°)5d ^{3}K°	3 (^{4}I°)5d ^{3}K°
		7	16 952.835(8)	2(0)	–29	–32	0.914	97 (^{4}I°)5d ^{5}L°	2 (^{2}H2°)5d ^{3}K°	1 (^{4}I°)5d ^{3}K°
		8	18 861.064(7)	4(1)	–12	26	1.043	99 (^{4}I°)5d ^{5}L°	1 (^{2}H2°)5d ^{3}K°	
		9	20 859.732(8)	2(0)	1	74	1.133	99 (^{4}I°)5d ^{5}L°		
		10	22 932.276(9)	1(0)	11	61	1.200	99 (^{4}I°)5d ^{5}L°	1 (^{2}K°)5d ^{3}M°	
		⋮	⋮	⋮	⋮	⋮	⋮	⋮	⋮	⋮
$4f^3(^4I°)6s$	$(\frac{9}{2},\frac{1}{2})°$	4	29 873.222(6)	5(1)	15	–1108	0.607	96 (^{4}I°)6s $(\frac{9}{2},\frac{1}{2})°$	2 (^{2}H°)6s $(\frac{9}{2},\frac{1}{2})°$	1 (^{4}G°)5d $(\frac{5}{2},\frac{3}{2})°$
		5	30 593.085(5)	7(0)	25	–999	0.903	74 (^{4}I°)6s $(\frac{9}{2},\frac{1}{2})°$	12 (^{4}I°)6s $(\frac{11}{2},\frac{1}{2})°$	3 (^{4}F°)5d $(\frac{5}{2},\frac{5}{2})°$
		⋮	⋮	⋮	⋮	⋮	⋮	⋮	⋮	⋮
$4f^3(^4I°)6p$	^{5}K	5	60 526.067(5)	14(0)	14	321	0.719	71 (^{4}I°)6p ^{5}K	22 (^{4}I°)6p ^{3}I	3 (^{4}I°)6p ^{5}I
		6	62 520.646(5)	15(0)	21	358	0.941	67 (^{4}I°)6p ^{5}K	17 (^{4}I°)6p ^{3}I	9 (^{4}I°)6p ^{5}I
		7	64 622.006(5)	15(2)	12	373	1.083	57 (^{4}I°)6p ^{5}K	20 (^{4}I°)6p ^{5}I	12 (^{4}I°)6p ^{3}K
		8	68 302.664(7)	11(0)	18	524	1.168	62 (^{4}I°)6p ^{5}K	21 (^{4}I°)6p ^{5}I	17 (^{4}I°)6p ^{3}K
		9	70 141.009(8)	6(0)	9	483	1.221	99 (^{4}I°)6p ^{5}K	1 (^{2}K°)6p ^{3}L	
		⋮	⋮	⋮	⋮	⋮	⋮	⋮	⋮	⋮

Notes. The first 3 columns are the configuration, term, and J value assignments for the level, parent terms of the $4f^3$ core electrons are in parentheses, any number following a term symbol is used to distinguish recurrent terms of equivalent electrons, and a ° following a term symbol indicates a term of odd parity. The fourth column is the optimised energy and its associated uncertainty in parentheses in units represented by the final decimal place of the energy value, the fifth column lists the number of lines classified for each level in the Nd–Ar PDL FT spectra, the number in parentheses is the number of blended or weak lines omitted from the level energy optimisation. The sixth and seventh columns are the differences between observed and calculated values of the present work using the parameterised Cowan code and of Gaigalas et al. (2019), respectively. The remaining columns list the Landé g-factors and three leading eigenvector percentages calculated using the Cowan code in this work. The level energies are optimised using LOPT using all 579 classified transitions listed in Table 4. The full version of this table is available at the CDS.

Level energies from the parameterised Cowan code calculations of this work generally differed by less than 50 cm^{-1} from the observed levels used to fit the radial integrals. This deviation is expected to be up to a few times larger for the remaining experimentally unknown levels of the $4f^4$, $4f^3 5f$, $4f^3 6s$, and $4f^3 6p$ configurations. In contrast, deviations of observed level energies from Gaigalas et al. (2019) calculations were 1 or 2 orders larger in size but still on average within a few percent. Due to the increasing level density at higher energies, a few percent difference in higher-lying level energies may lead to pronounced changes in the calculated eigenvector compositions and transition probabilities which are key to the empirical spectrum analysis. For example, mixing between the $4f^3 5d$ and $4f^3 6s$ configurations was evident between the $4f^3(^4G°)5d\ ^5I°_7$ and $4f^3(^4I°)6s\ (\frac{15}{2},\frac{1}{2})°_7$ levels. In Gaigalas et al. (2019), these two levels were predicted around 2000 cm^{-1} apart, which is an order of magnitude larger than the observed energy difference. Transition probabilities of $4f^3(^4G°)5d\ ^5I°_7$–$4f^3(^4I°)6p$ and $4f^4$–$4f^3(^4I°)6s\ (\frac{15}{2},\frac{1}{2})°_7$ from Gaigalas et al. (2019) were up to almost 3 orders of magnitude lower compared to those calculated by the parameterised Cowan code, which agree to an order of magnitude with the observed relative intensities.

5.1.2. Transitions classified in laboratory sources

All 432 Nd III transitions originating from the $4f^3 5d$, $4f^3 6s$, and $4f^3 6p$ configurations classified from the Nd–Ar PDL FT spectra are listed in Table 6. Around half of these transitions were measured with wavenumber uncertainties less than ±0.01 cm^{-1}, uncertainties above ±0.02 cm^{-1} were from weak lines around the noise level and constituted no more than 25% of this list. Similar to level energy uncertainty estimation in Sect. 5.1.1, the estimated systematic shifts from each of the six spectra were added in quadrature with the Ritz wavenumber uncertainty from the level optimisation to yield the final Ritz uncertainties (Kramida 2011) listed in Col. 6 of Table 6. Out of the 432 lines, 84 were found to be blended or too weak for reliable line fitting, these were excluded from the level optimisation but the differences between their observed and Ritz wavenumbers do not exceed 0.6 times their FWHM.

All Nd III lines below 3250 Å classified in the Nd–Ar PDL FT spectra from Table 6 were observed in the Nd VS grating spectra. Additionally, 191 of the $4f^3 5d$ – $4f^3 6p$ and $4f^3 6s$ – $4f^3 6p$ transitions with $g_u A < 10^8$ s^{-1} unobserved in the Nd–Ar PDL FT spectra were present in the Nd VS grating spectra, and these are listed in Table 7. For convenience, the $g_u A$ values are given in 10^6 s^{-1} to compare with the observed grating line intensities and

Table 6. Classified transitions of Nd III originating from the $4f^3 5d$, $4f^3 6s$, and $4f^3 6p$ configurations in the Nd–Ar PDL FT spectra (extract).

S/N	Int.	g_uA	$\log(g_lf)$	$FWHM$	σ_{obs}	σ_{Ritz}	$\sigma_{obs}-\sigma_{Ritz}$	λ^{air}_{Ritz}	Lower level		Upper level		E_l	E_u	Note
	(arb.)	(s^{-1})		(cm^{-1})	(cm^{-1})	(cm^{-1})	(cm^{-1})	(Å)	Config.	$Term_J$	Config.	$Term_J$	(cm^{-1})	(cm^{-1})	
(1)	(2)	(3)	(4)	(5)	(6)	(7)	(8)	(9)	(10)	(11)	(12)	(13)	(14)	(15)	(16)
10	120	1.3×10^7	–2.14	0.251	51 599.527(28)	51 599.538(9)	–0.011	1937.3641(3)	$4f^3(^4I°)5d$	$^5L°_8$	$4f^3(^4I°)6p$	$^3I_7$	18 861.064	70 460.602	B/W
5	68	6.1×10^8	–0.42	0.259	49 192.654(29)	49 192.658(8)	–0.004	2032.1699(3)	$4f^3(^4I°)5d$	$^5L°_6$	$4f^3(^4I°)6p$	$^3I_5$	15 158.154	64 350.812	
8	36	5.0×10^8	–0.51	0.177	48 981.473(32)	48 981.477(6)	–0.004	2040.9327(2)	$4f^3(^4I°)5d$	$^5K°_5$	$4f^3(^4I°)6p$	$^5H_4$	15 262.437	64 243.914	
5	32	7.4×10^8	–0.32	0.158	48 402.467(24)	48 402.455(7)	0.012	2065.3510(3)	$4f^3(^4I°)5d$	$^5K°_9$	$4f^3(^4I°)6p$	$^3K_8$	22 197.115	70 599.570	
6	40	6.5×10^8	–0.38	0.179	48 096.502(21)	48 096.490(6)	0.012	2078.4914(3)	$4f^3(^4I°)5d$	$^5K°_8$	$4f^3(^4I°)6p$	$^3K_7$	20 410.897	68 507.387	
13	90	9.2×10^8	–0.22	0.159	48 070.793(10)	48 070.798(7)	–0.005	2079.6024(3)	$4f^3(^4I°)5d$	$^5L°_7$	$4f^3(^4I°)6p$	$^5H_6$	16 952.835	65 023.633	
13	110	2.5×10^9	0.21	0.193	47 943.883(10)	47 943.894(8)	–0.011	2085.1076(3)	$4f^3(^4I°)5d$	$^5K°_9$	$4f^3(^4I°)6p$	$^5K_9$	22 197.115	70 141.009	
8	64	1.1×10^9	–0.14	0.221	47 891.776(17)	47 891.767(7)	0.009	2087.3774(3)	$4f^3(^4I°)5d$	$^5K°_8$	$4f^3(^4I°)6p$	$^5K_8$	20 410.897	68 302.664	
7	42	4.8×10^8	–0.50	0.166	47 856.459(17)	47 856.449(7)	0.010	2088.9181(3)	$4f^3(^4I°)5d$	$^5L°_8$	$4f^3(^4I°)6p$	$^5H_7$	18 861.064	66 717.513	
3	28	2.8×10^8	–0.74	0.275	47 840.961(53)	47 840.953(6)	0.008	2089.5948(3)	$4f^3(^4I°)5d$	$^5K°_7$	$4f^3(^4I°)6p$	$^5I_7$	18 656.272	66 497.225	
7	56	5.7×10^8	–0.43	0.233	47 795.548(20)	47 795.540(6)	0.008	2091.5805(2)	$4f^3(^4I°)5d$	$^5K°_7$	$4f^3(^4I°)6p$	$^3K_6$	18 656.272	66 451.812	
15	140	1.4×10^9	–0.03	0.214	47 636.162(10)	47 636.161(8)	0.001	2098.5793(3)	$4f^3(^4I°)5d$	$^5L°_8$	$4f^3(^4I°)6p$	$^5I_7$	18 861.064	66 497.225	
26	190	3.3×10^9	0.34	0.224	47 442.932(7)	47 442.932(7)	0.000	2107.1276(3)	$4f^3(^4I°)5d$	$^5L°_9$	$4f^3(^4I°)6p$	$^5K_8$	20 859.732	68 302.664	
⋮	⋮	⋮	⋮	⋮	⋮	⋮	⋮	⋮	⋮	⋮	⋮	⋮	⋮	⋮	
39	2000	1.1×10^7	–1.17	0.150	15 578.912(4)	15 578.909(4)	0.003	6417.1610(14)	$4f^4$	$^3K2_6$	$4f^3(^2H2°)5d$	$^3K°_6$	14 064.277	29 643.186	
15	910	7.1×10^6	–1.34	0.123	15 322.669(10)	15 322.666(7)	0.003	6524.4769(28)	$4f^4$	$^3K2_8$	$4f^3(^2H2°)5d$	$^3K°_7$	16 459.136	31 781.802	
12	800	5.9×10^5	–2.42	0.128	15 317.632(13)	15 317.640(4)	–0.008	6526.6177(15)	$4f^4$	$^5I_8$	$4f^3(^4I°)5d$	$^5K°_8$	5093.257	20 410.897	
312	21 000	5.8×10^6	–1.43	0.178	15 262.437(2)	15 262.437(2)	0.000	6550.2241(9)	$4f^4$	$^5I_4$	$4f^3(^4I°)5d$	$^5K°_5$	0.000	15 262.437	
12	820	6.3×10^5	–2.37	0.141	14 941.721(13)	14 941.724(3)	–0.003	6690.8208(13)	$4f^4$	$^5I_7$	$4f^3(^4I°)5d$	$^5K°_7$	3714.548	18 656.272	
5	220	2.3×10^6	–1.80	0.089	14 822.931(26)	14 822.913(6)	0.018	6744.4506(26)	$4f^4$	$^5G_5$	$4f^3(^2H2°)5d$	$^3G°_4$	18 313.004	33 135.917	B/W
13	1000	1.9×10^6	–1.88	0.145	14 715.629(12)	14 715.620(9)	0.009	6793.6253(40)	$4f^4$	$^5F_3$	$4f^3(^4I°)5d$	$^3G°_4$	11 424.605	26 140.225	
12	1000	4.5×10^5	–2.50	0.136	14 550.517(13)	14 550.524(7)	–0.007	6870.7090(34)	$4f^4$	$^5I_6$	$4f^3(^4I°)5d$	$^5K°_6$	2387.544	16 938.068	
6	590	3.2×10^6	–1.64	0.151	14 489.386(13)	14 489.379(5)	0.007	6899.7035(22)	$4f^4$	$^3K2_7$	$4f^3(^2H2°)5d$	$^3K°_6$	15 153.807	29 643.186	
4	430	2.3×10^5	–2.76	0.134	14 124.631(17)	14 124.643(3)	–0.012	7077.8735(15)	$4f^4$	$^5I_5$	$4f^3(^4I°)5d$	$^5K°_5$	1137.794	15 262.437	
11	2500	6.3×10^6	–1.28	0.130	13 460.188(15)	13 460.183(8)	0.005	7427.2738(46)	$4f^4$	$^5F_5$	$4f^3(^4I°)5d$	$^5G°_6$	13 210.278	26 670.461	
6	1200	1.8×10^6	–1.80	0.110	13 117.264(12)	13 117.264(12)	0.000	7621.4430(70)	$4f^4$	$^5F_2$	$4f^3(^4I°)5d$	$^3G°_3$	10 773.962	23 891.226	
4	2000	3.8×10^6	–1.45	0.187	12 697.081(22)	12 697.085(11)	–0.004	7873.6573(68)	$4f^4$	$^5F_4$	$4f^3(^4I°)5d$	$^5G°_5$	12 181.327	24 878.412	

Notes. (1) Signal-to-noise ratio, (2) approximate relative intensity corresponding to relative photon fluxes, (3)–(4) weighted transition probability and log of the weighted (absorption) oscillator strength calculated using the Cowan code, where g_u and g_l refer to statistical weights of the upper and lower energy levels, respectively, (5) full width at half maximum of the fitted line, (6)–(7) observed wavenumber and Ritz wavenumber from level optimisation, (8) wavenumber difference between observed and Ritz values, (9) air Ritz wavelength converted using the three-term dispersion formula from Peck & Reeder (1972), (10)–(13) energy levels associated with the transition, their energies are in Cols. (14)–(15), respectively, and (16) contains comments of the observed transition, where 'B/W' indicates a blended or weak line with unreliable wavenumber and intensity, which was omitted from level optimisation. Standard uncertainties of values in Cols. (6), (7), and (9) are in parentheses in units of the final decimal place. The full version of this table is available at the CDS.

Table 7. Transitions of Nd III originating from the $4f^3 6s$ and $4f^3 6p$ configurations observed only in the Nd VS grating spectra (extract).

Int.	$g_u A$ (10^6 s^{-1})	$\log(g_l f)$	λ_{obs} (Å)	λ_{Ritz} (Å)	λ^{air}_{Ritz} (Å)	Lower level	Upper level	E_l (cm^{-1})	E_u (cm^{-1})
(1)	(2)	(3)	(4)	(5)	(6)	(7)	(8)	(9)	(10)
32	160	–1.06	1904.916	1904.9130(7)	1904.2801	$4f^3(^4I^\circ)5d\ ^5H^\circ_3$	$4f^3(^4F^\circ)6p\ ^5G_2$	19 593.094	72 088.930
39	210	–0.94	1906.218	1906.2183(11)	1905.5852	$4f^3(^4I^\circ)5d\ ^3K^\circ_6$	$4f^3(^4F^\circ)6p\ ^5G_5$	23 120.073	75 579.962
7	65	–1.44	1933.861	1933.8594(11)	1933.2223	$4f^3(^4I^\circ)5d\ ^3H^\circ_4$	$4f^3(^4F^\circ)6p\ ^5G_3$	21 491.882	73 201.950
10	55	–1.50	1950.555	1950.5562(6)	1949.9165	$4f^3(^4I^\circ)5d\ ^5I^\circ_6$	$4f^3(^2H2^\circ)6p\ ^3I_5$	21 980.522	73 247.950
11	97	–1.25	1977.631	1977.6266(10)	1976.9825	$4f^3(^4I^\circ)5d\ ^5G^\circ_6$	$4f^3(^2H2^\circ)6p\ ^1I_6$	26 670.461	77 236.125
⋮	⋮	⋮	⋮	⋮	⋮	⋮	⋮	⋮	⋮
76	44	–1.17	3183.563	3183.5630(13)	3182.6426	$4f^3(^4F^\circ)5d\ ^5G^\circ_6$	$4f^3(^4I^\circ)6p\ ^5K_7$	33 210.660	64 622.006
63	32	–1.31	3190.919	3190.9164(12)	3189.9940	$4f^3(^4F^\circ)5d\ ^5G^\circ_6$	$4f^3(^4I^\circ)6p\ ^5I_6$	33 210.660	64 549.620
50	34	–1.28	3200.866	3200.8665(5)	3199.9417	$4f^3(^2H2^\circ)5d\ ^3I^\circ_5$	$4f^3(^4I^\circ)6p\ ^5I_4$	29 397.423	60 638.963
39	17	–1.58	3212.476	3212.4753(6)	3211.5475	$4f^3(^2H2^\circ)5d\ ^3I^\circ_5$	$4f^3(^4I^\circ)6p\ ^5K_5$	29 397.423	60 526.067
69	190	–0.53	3213.624	3213.6268(9)	3212.6987	$4f^3(^4I^\circ)6s\ (\frac{13}{2},\frac{1}{2})^\circ_7$	$4f^3(^4I^\circ)6p\ ^5H_6$	33 906.143	65 023.633

Notes. (1) Approximate relative intensity corresponding to relative energy flux, (2)–(3) weighted transition probability and log of the weighted (absorption) oscillator strength calculated using the Cowan code, where g_u and g_l refer to statistical weights of the upper and lower energy levels, respectively, (4) observed vacuum wavelength of the line with minimum uncertainty at ±0.006 Å estimated for unblended and symmetric lines of moderate intensity, (5) vacuum Ritz wavelength resulting from the level optimisation, its standard uncertainty is in parentheses in units of the final decimal place, (6) air Ritz wavelength converted using the three-term dispersion formula from Peck & Reeder (1972), (7)–(10) information on energy levels associated with the transition. The full version of this table is available at the CDS.

could be roughly compared with intensities from the FT spectra. The relative intensities generally followed the $g_u A$ values, which is remarkable for these weak lines originating from the overall highly mixed $4f^3 6p$ levels. These lines were not used in level energy estimation, their uncertainties were too large, preventing them from significantly contributing to the optimised level energies. For the ten $4f^3 6p$ levels above 72 000 cm^{-1}, level energy uncertainties could be lowered slightly with the inclusion of Nd VS grating wavelengths due to low line counts and low S/N in the FT spectra, but the lowest grating spectra uncertainties are still three times the largest uncertainties of the FT spectral lines. Unlike the Nd–Ar PDL FT spectra, the Nd VS grating spectra were very line-rich in this spectral region with around 10^4 measured lines, therefore uncertainty improvements using the grating lines would also not be guaranteed due to widespread line blending. The Ritz wavelength uncertainties of these lines were estimated using the LOPT program by assigning them zero weights in the level optimisation.

5.2. Methodology of analysis

The empirical spectrum analysis of complex atomic structures involves the classification of spectral lines belonging to the experimentally unknown energy levels of interest, primarily by matching theoretical and experimental relative intensity patterns at wavenumbers expected from theoretical level energies and energy separations.

With accurate transition probability calculations, one can expect the observed relative line intensities to be similar to those calculated for the corresponding transitions. For example, the eighth and final rows of the top half of Table 6 are two lines at 47 891.776 cm^{-1} and 47 442.932 cm^{-1} originating from the upper level $4f^3(^4I^\circ)6p\ ^5K_8$, with observed relative intensities matching their theoretical branching ratios of $g_u A$. Similarly, the final three rows of the bottom half of Table 6 show good agreement between the ratios of their $g_u A$ values and the ratios of their observed relative intensities, as the three lines were all in the same spectrum and have upper levels at similar energies.

To begin the analysis, a few energy levels of the ground and lowest-lying configurations must be established for an atom. This usually involves classifying the corresponding transitions which tend to be of the highest intensities and/or are self-absorbed in the discharge conditions that best populate these energy levels of the atom. The classification of these transitions is also often approached by looking for repeated wavenumber separations of observed lines (e.g. see the end of Chapter 1 of Cowan 1981). Then, the level system could be expanded level by level by matching the expected intensity pattern and wavenumbers of lines connecting an unknown level to the known levels.

Due to the immense number of spectral lines observed from complex atoms, the number of ambiguous matches for a particular intensity pattern rises exponentially with increasing experimental and theoretical wavenumber uncertainties. This issue escalates further when looking for low-intensity lines, which tend to be much more common and have higher uncertainties in both wavenumber and intensity. The solution then is to find corroboration with other available experimental evidence; in the analysis of Nd III, the correct lines for transitions connecting a potential new level should:

1. match the energy differences between known levels and the level of interest, within a tolerance around the order of observed wavenumber uncertainties (0.05 cm^{-1} was suitable in most cases as it was around the upper-bound of wavenumber uncertainties of the Nd–Ar PDL FT spectra line list),
2. satisfy the E1 transition selection rules in the absence of external fields (i.e. change of parity and $\Delta J = 0 \pm 1$ but not $J = 0 \leftrightarrow 0$),
3. be within the expected wavenumber range, subject to the accuracy of theoretical level energy predictions,
4. show agreement between observed and predicted relative intensity patterns,
5. correspond to a tentative energy level which would enable the establishment of other experimentally unknown levels from classifying transitions connecting to this tentative level,

6. have the expected isotope and/or hyperfine structure line profiles,
7. have the expected relative intensities at different thermal conditions (e.g. in stars, the cooler HCL or hotter VS discharges),
8. have the expected Zeeman patterns in stellar spectra or other suitable light sources using theoretical Landé g-factors,
9. and not be lines from other atomic species.

In most cases, not all of the above conditions could be satisfied; the first four were generally considered necessary and the rest served as evidence for more confident classifications, which were subject to data availability. An energy level could also be established with only one line if the said line satisfied many of these conditions without ambiguities. The first three conditions were written as a computer program (similar to Azarov et al. 2018) to filter all observed wavenumbers to generate candidate level energies and their corresponding sets of candidate lines. Newly established energy levels were also used to empirically improve the theoretical Cowan code calculations as the analysis progressed, which reduced the wavenumber and relative intensity search ranges.

The described methodology greatly depends on the completeness, spectral range, and accuracy of the observed wavenumbers and relative intensities. From the discussion in Sect. 4, the ubiquity of blended and weak lines of Nd could prevent the detection of crucial transitions or force an increase of uncertainty tolerances, resulting in an unresolvable number of ambiguous matches. The present work reached its conclusion due to this reason.

5.3. Revision of previously published energy levels

The analysis began with the assumption of the correct establishment of the ground term, $4f^4\ {}^5I$, by H. M. Crosswhite (Martin et al. 1978). This became more evident and was concluded indeed correct as the analysis progressed; the 5 levels of the $4f^4\ {}^5I$ term enabled the identification of more than 200 interconnected levels of the 4f-excited configurations up to nl = 5f, consistent with observed spectra, isotope structure line profiles, and parameterised Cowan code calculations.

The immediate search for the 24 levels of the $4f^35d$ configuration from Martin et al. (1978) was aided by calculations from Zhang et al. (2002), Ryabchikova et al. (2006) and Gaigalas et al. (2019). Of the 35 $4f^35d$ levels proposed by Ryabchikova et al. (2006) all were confirmed except for the $4f^3(^4I^\circ)5d\ {}^5H^\circ_3$ level, which was revised using its transition to the ground level classified at 19 593.094 cm^{-1} and transitions from $4f^3(^4I^\circ)6p\ {}^5I_4$ and $4f^3(^4I^\circ)6p\ {}^5H_3$. A positive wavenumber shift of order 0.01 cm^{-1} exists for most energy levels and transitions observed in this work compared to those of Aldenius (2001) and Ryabchikova et al. (2006). This was from the use of COG values to account for the observed Nd III isotope line profiles, rather than the peak wavenumbers used by Aldenius (2001) which did not consider isotope shifts of energy levels in wavenumber measurements.

5.4. Searching for previously unknown energy levels

5.4.1. $4f^3(^4I^\circ)$ sub-configuration

Theoretical calculations from Ryabchikova et al. (2006) and Gaigalas et al. (2019) aided the complete identification of all 40 levels of the $4f^3(^4I^\circ)5d$, all 29 levels of the $4f^3(^4I^\circ)6p$, and all 8 levels $4f^3(^4I^\circ)6s$ sub-configurations. Despite the $4f^4\ {}^5I$–$4f^3(^4I^\circ)5d$ transitions lying within the line-rich and blend-rich visible regions, their classifications were possible due to their high relative intensities and the large number of $4f^3(^4I^\circ)5d$–$4f^3(^4I^\circ)6p$ transitions observed and straightforwardly classified in the line-sparse and generally blend-free UV region.

5.4.2. $4f^3(^4G^\circ)5d$ levels and Cowan code calculations

A group of lines with the highest S/Ns in spectrum E around 35 500 cm^{-1} showed the $4f^4$–$4f^35d$ isotope profile and resembled relative intensities of the $4f^4\ {}^5I$–$4f^3(^4G^\circ)5d\ {}^5H^\circ$ transitions predicted from Gaigalas et al. (2019). All of the $4f^3(^4G^\circ)5d\ {}^5H^\circ$ levels were found around 2500 cm^{-1} below the energies calculated in Gaigalas et al. (2019), this offset was then expected for the other $4f^3(^4G^\circ)5d$ levels, which led to the classification of weaker $4f^4\ {}^5I$–$4f^3(^4G^\circ)5d$ transitions from a few levels of the $4f^3(^4G^\circ)5d\ {}^5G^\circ$ and $4f^3(^4G^\circ)5d\ {}^5I^\circ$ terms.

At this stage, many observable levels predicted by Gaigalas et al. (2019) appeared highly mixed, which was indicated by their missing or multiply assigned LS-coupling labels. Parameterised Cowan code calculations were then performed including the new levels established for the $4f^3(^4I^\circ)5d$, $4f^3(^4I^\circ)6s$, $4f^3(^4I^\circ)6p$, and $4f^3(^4G^\circ)5d$ sub-configurations. LS labels of a handful of $4f^35d$ levels were re-assigned using the newly calculated eigenvector compositions, and the improved transition probabilities enabled the identification of more $4f^35d$ levels. All of these were assigned to the $4f^3(^4F^\circ)5d$, $4f^3(^2H2^\circ)5d$, $4f^3(^4G^\circ)5d$, and $4f^3(^2K^\circ)5d$ sub-configurations. Remaining transitions of the experimentally unknown $4f^35d$ levels to the ground term $4f^4\ {}^5I$ were expected to be very weak in the PDL spectrum, so the focus shifted to identifying other low-lying levels of the $4f^4$ configuration.

5.4.3. $4f^4$ levels

Levels of the low-lying ^5F, ^5G, $^3H4$, and $^3K2$ terms of the $4f^4$ configuration were identified, their transitions from the $4f^35d$ levels are generally much weaker and lie within the most line-rich spectral regions in the visible. Isotope profiles and relative intensities of these transitions were much more uncertain due to low S/Ns and high chances of significant line blending. Cowan code calculations were also less well constrained for the $4f^4$ configuration due to the lack of identified levels of this configuration. This was the final and most lengthy stage of the analysis, where corroboration with Nd VS and stellar grating spectra became vital.

Initially, progress was made identifying $4f^4\ {}^5G_5$, where five lines observed in the Nd–Ar PDL spectrum (four of which were at S/Ns less than 10, two of which were blended) were supported by the spectral syntheses of HD 170973 and HD 144893 using transition probabilities and Landé g-factors predicted by the Cowan code. A nearly blend-free example is shown in Fig. 5 containing the $4f^4\ {}^5G_5$–$4f^3(^4G^\circ)5d\ {}^5G^\circ_6$ transition (S/N 5 in the Nd–Ar PDL FT spectrum) at 4693.88 Å, where corroboration with stellar spectra is also shown for the later classified transition of $4f^4\ {}^5F_5$–$4f^3(^4F^\circ)5d\ {}^5F^\circ_5$ at 4693.32 Å. The average Nd abundance from four mostly blend-free $4f^4\ {}^5G_5$ lines in the spectrum of HD 170973 was estimated at $\log \varepsilon_{\rm Nd} = 5.65 \pm 0.09$, in agreement with the reference value 5.63 ± 0.14 (see Sect. 3.4). Except for the 4693.88 Å line, all lines of $4f^4\ {}^5G_5$ in the spectrum of HD 144897 were blended by Zeeman components of nearby lines, but three of them provided an abundance estimate at $\log \varepsilon_{\rm Nd} = 5.66 \pm 0.13$, which again was in agreement with average Nd abundance 5.59 ± 0.20 derived in this star by Ryabchikova et al. (2006) from other Nd III lines.

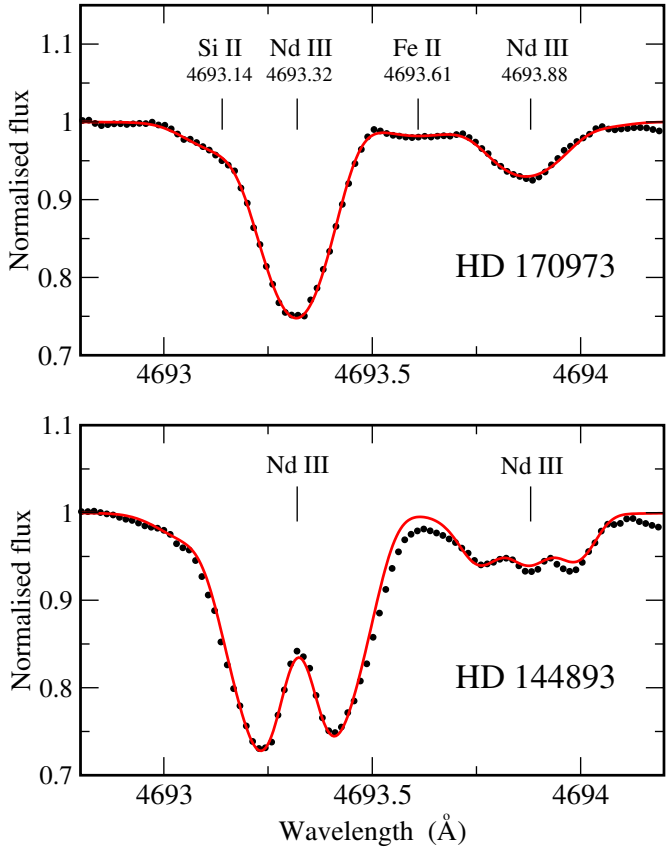

Fig. 5. Observed (black dotted line) and synthesised (red line) spectra in the interval 4692.5–4694.5 Å of HD 170973 and HD 144893 with surface magnetic fields $\langle B_z \rangle$<1 kG and $\langle B_z \rangle$=8.8 kG, respectively, containing two newly classified transitions of Nd III: $4f^4\ {}^5F_5$–$4f^3({}^4F^\circ)5d\ {}^5F^\circ_5$ at 4693.32 Å and $4f^4\ {}^5G_5$–$4f^3({}^4G^\circ)5d\ {}^5G^\circ_6$ at 4693.88 Å.

Such abundance estimates greatly supported the identification of $4f^4\ {}^5G_5$ and other $4f^4$ levels.

The classification of transitions to $4f^4\ {}^5G_5$ provided a useful guide on the expected relative intensities and S/Ns of transitions from $4f^3$5d to other nearby low-lying $4f^4$ levels observed in the Nd–Ar PDL spectra. Subsequently, the $4f^4\ {}^3K2_{6,7}$ and $4f^4\ {}^5F_5$ levels were confidently identified with support from H. M. Crosswhite's list of 643 unclassified Nd III lines. Most notably, these lines from her sliding spark grating spectra indicated several transitions that were weak, blended, and/or not fitted in the Nd–Ar PDL spectra. The four levels belonging to three separate terms of the $4f^4$ configuration improved our Cowan code parameterisation, and the identifications of $4f^4\ {}^3K2_8$, $4f^4\ {}^5G_{3,4}$, and $4f^4\ {}^3H4_5$ followed with confirmations from stellar spectra, which also enabled the identification of more levels of the $4f^3({}^4F^\circ)5d$, $4f^3({}^2H2^\circ)5d$, $4f^3({}^4G^\circ)5d$ and $4f^3({}^4D^\circ)5d$ sub-configurations.

Identification of the $4f^4\ {}^5F_{2,3,4}$ levels proved more challenging. The transitions $4f^4\ {}^5F_J$–$4f^3({}^4S^\circ)5d\ {}^5D^\circ_{J-1}$ ($J > 1$) were tentatively classified prior to the establishment of their energy levels, using their high intensities, isotope profiles, agreement in intensity and wavenumber with calculations, and presence in H. M. Crosswhite's unclassified Nd III line list and the stars. However, the $4f^4\ {}^5F_J$–$4f^3({}^4S^\circ)5d\ {}^5D^\circ_J$ transitions were expected around the noise level in the Nd–Ar PDL FT spectra with too many ambiguous classifications, so levels of the $4f^4\ {}^5F$ and $4f^3({}^4S^\circ)5d\ {}^5D^\circ$ terms could not be established using only the transitions between the two terms. In looking for other evidence to resolve these ambiguities, the $4f^3({}^4F^\circ)6p\ {}^5G_{2,3,4,5}$ levels proved useful, which were established using the VS grating spectra with the strongest lines to $4f^3({}^4F^\circ)5d\ {}^5H^\circ_{3,4,5,6}$ also observed in the Nd–Ar PDL FT spectrum (the same approach was used in establishing the $4f^3({}^2H2^\circ)6p$ levels). The $4f^3({}^4F^\circ)6p\ {}^5G$ levels aided the identification of the $4f^3({}^4F^\circ)5d\ {}^5F^\circ_{2,3,4}$ levels which have transitions to $4f^4\ {}^5F_{2,3,4}$ observed at intermediate S/Ns. Even when additionally considering transitions from $4f^3({}^4F^\circ)5d\ {}^5F^\circ_{2,3,4}$, several attempts were made at classifying the $4f^4\ {}^5F_{2,3,4}$–$4f^3$5d transitions in the Nd–Ar PDL spectra before an agreement could be reached with lines observed in the stellar spectra.

6. Outlook

This extended analysis of the four low-lying configurations $4f^4$, $4f^3$5d, $4f^3$6s, and $4f^3$6p of Nd III will enable laboratory measurements of their lifetime and branching fractions for accurate determination of transition probabilities. The experimentally established energy levels will improve future atomic structure calculations of Nd III by serving as benchmarks and semi-empirical constraints.

Attempts to identify levels of the doubly excited configurations of Nd III were unsuccessful as the strongest predicted transitions originating from $4f^2$5d^2 are to the still unknown levels of the $4f^3$5d configuration. The remaining unknown $4f^4$–$4f^3$5d transitions are expected to be very weak in the recorded Nd–Ar PDL FT spectra, with too many ambiguities in the expected intensity patterns and wavenumber ranges. Further large-scale experimental investigations of Nd III atomic structure would require alternatives or extensions of the presented experimental and analytical methods, such as altering Nd discharge conditions to better populate higher-lying Nd III energy levels and to separate Nd III lines from other species, and/or establishing isolated energy level systems with strong lines which would eventually be connected to the current network of levels and ultimately to the ground level.

From inspecting the Nd VS spectrum of the 390–1525 Å region, a group of strong lines lying around 450 Å were found to potentially correspond to the $5p^64f^4$–$5p^54f^4$5d transitions. Due to limited computational resources, attempts to account for the $4f^4 \leftrightarrow 5p^54f^5$ and $5p^64f^3$5d $\leftrightarrow 5p^54f^4$5d interactions required the omission of the $4f^3$7s, $4f^3$6d, $4f^3$5f, and the doubly excited configurations in the interaction space of the calculations of Table 1. Calculations using this new interaction space with 5p-excited configurations resulted in a reduction of transition probabilities of the $4f^4$–$4f^3$5d transitions by a factor of around 0.6, but changes in branching ratios were not significant enough to invalidate line classifications of the present work. The reduction in transition probability is similar to Nd IV (Arab et al. 2019) and Nd V (Deghiche et al. 2015). Therefore, future experimental validation of levels predicted to involve the 5p core-excitation of Nd III should also improve semi-empirical transition probability calculations.

Energy levels belonging to the $4f^3({}^4I^\circ)6d$ and $4f^3({}^4I^\circ)7s$ sub-configurations have been identified using the Nd–Ar PDL FT spectra together with aid from the Nd VS grating spectra. They lie about 6000 cm^{-1} lower than predicted by Gaigalas et al. (2019). Levels of the $4f^3$5f configuration are also being established from the classification of the $4f^3$5d – $4f^3$5f transitions in another set of Nd grating spectra recorded in the range 820–1159 Å. These results, totaling more than 100 energy levels, are being prepared for publication, where the energy level and transition probability calculations using Cowan's codes will also be included in full.

Many energy levels of Nd I–III remain unknown experimentally, as more than 10^4 lines are still unclassified in the Nd–Ar PDL spectra, these are expected to be mostly from Nd II. The Penning discharge lamp design has shown to be a suitable source of Nd spectra, with particular enhancements of Nd II and Nd III populations compared to the alternative HCL at running conditions which maximised the Nd III resonance line intensities. For further investigations of Nd and other lanthanide elements, high-resolution spectroscopy of a variety of plasma discharges, accurate semi-empirical atomic structure calculations, and rigorous line list extraction methods are emphasised to be key strategies.

7. Summary

Supplemented by atomic structure calculations, Nd–Ar HCL FT spectra, Nd VS grating spectra, and Nd-rich stellar spectra, 144 energy levels of Nd III have been determined from the classification of 432 Nd III transitions measured by FT spectroscopy of a Nd–Ar PDL between 11 500–54 000 cm^{-1} (8695–1852 Å), 39 previously published energy levels were confirmed and 105 new levels of the $4f^4$, $4f^35d$, $4f^36s$, and $4f^36p$ configurations are reported here for the first time. These results are the most extensive and most accurate (to a few 10^{-3} cm^{-1}) Nd III energy level and transition wavenumber data to date, which will support theoretical atomic structure investigations of the lanthanides and enable wider and more reliable applications of Nd III atomic data in astronomy.

Acknowledgements. This work was supported by the STFC of the UK, grant numbers ST/S000372/1, ST/N000838/1, and ST/W000989/1, and the research project FFUU-2022–0005 of the Institute of Spectroscopy of the Russian Academy of Sciences. The authors are grateful to Dr J.-F. Wyart and Prof. W.-Ü. Tchang-Brillet for providing the Nd vacuum sliding spark grating plates recorded at NIST, and to Prof. C. R. Cowley for sharing the unpublished Nd III line lists of Dr H. M. Crosswhite. The authors would also like to thank Dr A. Kramida for his helpful comments on the manuscript.

References

Abbott, B. P., Abbott, R., Abbott, T., et al. 2017, Phys. Rev. Lett., 119, 161101
Aldenius, M. 2001, Master's Thesis, University of Lund, Sweden
Arab, K., Deghiche, D., Meftah, A., et al. 2019, J. Quant. Spectrosc. Radiat. Transf., 229, 145
Azarov, V. 1991, Preprint of the Institute of Spectroscopy (Troitsk: Russian Academy of Sciences), 1
Azarov, V., Kramida, A., & Vokhmentsev, M. Y. 2018, Comput. Phys. Commun., 225, 149
Berglund, M., & Wieser, M. E. 2011, Pure Appl. Chem., 83, 397
Blaise, J., Wyart, J.-F., Hoekstra, R., & Kruiver, P. 1971, J. Opt. Soc. Am., 61, 1335
Blaise, J., Wyart, J.-F., Djerad, M. T., & Ahmed, Z. B. 1984, Phys. Scr, 29, 119
Bord, D. 2000, A&AS, 144, 517
Brault, J. W. 1987, Microchim. Acta, 93, 215
Brewer, L. 1971, J. Opt. Soc. Am., 61, 1666
Clear, C. P., Pickering, J. C., Nave, G., Uylings, P., & Raassen, T. 2022, ApJS, 261, 35
Coulter, D., Foley, R., Kilpatrick, C., et al. 2017, Science, 358, 1556
Cowan, R. D. 1981, The Theory of Atomic Structure and Spectra (University of California Press)
Cowley, C. R., Ryabchikova, T., Kupka, F., et al. 2000, MNRAS, 317, 299
Davis, S. P., Abrams, M. C., & Brault, J. W. 2001, Fourier Transform Spectrometry (Elsevier)
Deghiche, D., Meftah, A., Wyart, J.-F., et al. 2015, Phys. Scr, 90, 095402
Dieke, G. H., & Crosswhite, H. 1963, Appl. Opt., 2, 675
Dieke, G., Crosswhite, H., & Dunn, B. 1961, J. Opt. Soc. Am., 51, 820
Domoto, N., Tanaka, M., Kato, D., et al. 2022, ApJ, 939, 8
Dzuba, V., Safronova, U., & Johnson, W. 2003, Phys. Rev. A, 68, 032503
Engström, L. 1998, GFit, A Computer Program to Determine Peak Positions and Intensities in Experimental Spectra. Tech. Rep. LRAP-232, Atomic Physics, Lund University
Even, W., Korobkin, O., Fryer, C. L., et al. 2020, ApJ, 899, 24
Finley, D. S., Bowyer, S., Paresce, F., & Malina, R. F. 1979, Appl. Opt., 18, 649
Fontes, C., Fryer, C., Hungerford, A., Wollaeger, R., & Korobkin, O. 2020, MNRAS, 493, 4143
Gaigalas, G., Kato, D., Rynkun, P., Radžiūtė, L., & Tanaka, M. 2019, ApJS, 240, 29
Haris, K., & Kramida, A. 2017, ApJS, 233, 16
Heise, C., Hollandt, J., Kling, R., Kock, M., & Kühne, M. 1994, Appl. Opt., 33, 5111
Johnson, D. A., & Nelson, P. G. 2017, J. Phys. Chem. Ref. Data, 46, 013109
Kasen, D., Badnell, N., & Barnes, J. 2013, ApJ, 774, 25
Kato, K.-I. 2003, PASJ, 55, 1133
Koczorowski, W., Stachowska, E., Furmann, B., et al. 2005, Spectrochim. Acta Part B, 60, 447
Kramida, A. 2011, Comput. Phys. Commun., 182, 419
Kramida, A. 2021, A suite of atomic structure codes originally developed by R. D. Cowan adapted for Windows-based personal computers, National Institute of Standards and Technology, https://doi.org/10.18434/T4/1502500
Kramida, A., Nave, G., & Reader, J. 2017, Atoms, 5, 9
Kramida, A., Ralchenko, Y., Reader, J., & the NIST ASD Team. 2022, NIST Atomic Spectra Database (version 5.10) (Gaithersburg, MD: National Institute of Standards and Technology)
Lawler, J., Schmidt, J., & Den Hartog, E. 2022, J. Quant. Spec. Radiat. Transf., 289, 108283
Learner, R., & Thorne, A. 1988, J. Opt. Soc. Am. B, 5, 2045
Liggins, F. S., Pickering, J. C., Nave, G., Ward, J. W., & Tchang-Brillet, W.-Ü. L. 2021, ApJS, 252, 10
Lodders, K. 2021, Space Sci. Rev., 217, 44
Martin, W. C., Zalubas, R., & Hagan, L. 1978, Atomic Energy Levels – The Rare-Earth Elements (US: Nat. Bur. Stand.), 422
Mashonkina, L., Ryabchikova, T., Ryabtsev, A., & Kildiyarova, R. 2009, A&A, 495, 297
Meftah, A., Wyart, J.-F., Sinzelle, J., et al. 2008, Phys. Scr, 77, 055302
Nave, G., & Johansson, S. 2012, ApJS, 204, 1
Nave, G., Johansson, S., Learner, R., Thorne, A., & Brault, J. 1994, ApJS, 94, 221
Nave, G., Griesmann, U., Brault, J. W., & Abrams, M. C. 2015, Astrophysics Source Code Library [record ascl:1511.004]
Palmeri, P., Quinet, P., Frémat, Y., Wyart, J.-F., & Biémont, E. 2000, ApJS, 129, 367
Peck, E. R., & Reeder, K. 1972, J. Opt. Soc. Am., 62, 958
Przybylski, A. 1977, MNRAS, 178, 71
Radziemski, L. J., & Andrew, K. L. 1965, J. Opt. Soc. Am., 55, 474
Ryabchikova, T., Ryabtsev, A., Kochukhov, O., & Bagnulo, S. 2006, A&A, 456, 329
Ryabchikova, T., Kochukhov, O., & Bagnulo, S. 2008, A&A, 480, 811
Ryabchikova, T., LeBlanc, F., & Shulyak, D. 2011, in Magnetic Stars, eds. D. O. Kudryavtsev, & I. I. Romanyuk, 69
Saloman, E. B. 2010, J. Phys. Chem. Ref. Data, 39, 033101
Silva, R. F., Sampaio, J. M., Amaro, P., et al. 2022, Atoms, 10, 18
Smartt, S., Chen, T.-W., Jerkstrand, A., et al. 2017, Nature, 551, 75
Stancik, A. L., & Brauns, E. B. 2008, Vib. Spectrosc., 47, 66
Tanaka, M., & Hotokezaka, K. 2013, ApJ, 775, 113
Tanaka, M., Kato, D., Gaigalas, G., et al. 2018, ApJ, 852, 109
Tanaka, M., Kato, D., Gaigalas, G., & Kawaguchi, K. 2020, MNRAS, 496, 1369
Thorne, A., Harris, C., Wynne-Jones, I., Learner, R., & Cox, G. 1987, J. Phys. E, 20, 54
Valenti, S., David, J., Yang, S., et al. 2017, ApJ, 848, L24
Watson, D., Hansen, C. J., Selsing, J., et al. 2019, Nature, 574, 497
Whaling, W., Anderson, W., Carle, M., Brault, J., & Zarem, H. 1995, J. Quant. Spec. Radiat. Transf., 53, 1
Whaling, W., Anderson, W., Carle, M., Brault, J., & Zarem, H. 2002, J. Res. Natl. Inst. Stand. Technol., 107, 149
Wyart, J.-F. 2010, Phys. Scr, 82, 035302
Wyart, J.-F., Meftah, A., Tchang-Brillet, W.-Ü. L., et al. 2007, J. Phys. B, 40, 3957
Wyart, J.-F., Tchang Brillet, W.-U., Ryabtsev, A. N., et al. 2010, Book of Abstracts, 7th International Conference on Atomic and Molecular Data and their Applications, Vilnius
Zhang, Z., Svanberg, S., Palmeri, P., Quinet, P., & Biémont, E. 2002, A&A, 385, 724